ADDIS ABABA UNIVERSITY

ADDIS ABABA INSTITUTE OF TECHNOLOGY

SCHOOL OF CIVIL AND ENVIRONMENTAL ENGINEERING

Geodesy and Geomatics Program

Evaluation of the Performance of Remote Sensing-based Drought Indices for Agricultural Drought Characterization: The case of Tigray Region, Northern Ethiopia

By

Haregeweyen Minas Kasaye

A Thesis Submitted to

School of Civil and Environmental Engineering in Partial Fulfillment of the Requirements for the Degree of Master of Science in Geodesy and Geomatics Program (Specialization in Geomatics Engineering)

March, 2022

Addis Ababa, Ethiopia

The undersigned have examined the thesis entitled "Evaluation of the Performance of Remote Sensing-based Drought Indices for Agricultural Drought Characterization: The case of Tigray Region, Northern Ethiopia" presented by Haregeweyen Minas, a candidate for the degree of Master of Science and hereby certify that it is worthy of acceptance.

Dr. Berhan Gessesse		
Advisor	Signature	Date
Internal Examiner	Signature	Date
External Examiner	Signature	Date
Chair person	Signature	Date

Declaration

I certify that this research work titled "Evaluation of the Performance of Remote Sensing-based Drought Indices for Agricultural Drought Characterization: The case of Tigray Region, Northern Ethiopia" is my own work. The work has not been presented elsewhere for assessment. Where material has been used from other sources it has been properly acknowledged / referred.

Haregeweyen Minas		
Name of Student	Signature	Date

As Master research advisor, I hereby certify that I have read and evaluated this MSc thesis prepared under my guidance.

Dr. Berhan Gessesse		
Name of the Advisor	Signature	Date

Acknowledgments

First, I thank the Almighty God for His unlimited blessings and for giving me the strength to complete this study.

I would like to express my deepest gratitude to my advisor, Dr. Berhan Gessesse, for his interest in my research work, for his excellent guidance, invaluable suggestions, and critical comments on this thesis.

I would like to thank Dire Dawa University for this higher education sponsorship and I acknowledge the Ethiopian Geospatial Information Institute, National Meteorological Agency, and the Central Statistical Agency for their support concerning the data required for the present study. Finally, my most appreciations are to my parents and friends for their encouragement and support.

Table of Contents

List of Figures

List of Tables

List of Abbreviations

CMI	Crop moisture index
CSA	Central Statistical Agency
DEVNDVI	NDVI deviation
DN	Digital Number
DOS	Dark Object Subtraction
DSI	Drought severity index
EROS	Earth Resources Observation and Science
ESI	Evaporative Stress Index
Eta	Actual evapotranspiration anomaly
ETM+	Enhanced Thematic Mapper plus
FLAASH	Fast Line-of-sight Atmospheric Analysis of Spectral Hypercubes
GII	Geospatial Information Institute
GIEWS	Global Information and Early Warning System
LP DAAC	Land Processes Distributed Active Archive Center
LST	Land Surface Temperature
MODIS	Moderate resolution imaging Spectroradiometer
NDVI	Normalized Difference Vegetation Index
NMA	National Meteorological Agency
NR	Normal ratio
OLI	Operational Land Imager

PET	Potential evapotranspiration
PSDI	Palmer drought severity index
Q / ha	quintal per hectare
QUAC	Quick Atmospheric Correction
SPEI	Standardized Precipitation and Evapotranspiration Index
SPI	Standardized precipitation index
SST	Sea Surface Temperature
SVI	Standardized Vegetation Index
SWI	Standardized Water Index
TCI	Temperature condition index
TIRS	Thermal Infrared Sensor
TM	Thematic Mapper
TOA	Top of Atmosphere
TVDI	Temperature vegetation dryness index
USGS	United State Geological Survey
UTM	Universal Transverse Mercator
VCI	Vegetation Condition Index
VDSI	Vegetation Drought Monitor Synthesized Index
VHI	Vegetation health index

List of Appendices

ABSTRACT

Evaluation of the Performance of Remote Sensing-based Drought Indices for Agricultural Drought Characterization: The case of Tigray Region, Northern Ethiopia

Haregeweyen Minas Kasaye

The increasing drought severities and consequent devastating effects on agriculture in the Tigray Region needs better monitoring of drought. For this purpose, numerous remote sensing-based drought indices have been proposed. However, the performance of remote sensing-based drought indices varies among regions and sensor characteristics. In addition, their different assumptions and data input requirements make it necessary to evaluate their suitability for drought monitoring before they become operational in a specific region. Using Landsat and MODIS images in the Tigray Region, this study assesses and compares the efficacy of four remote sensing-based drought indices for agricultural drought characterization. Drought indices investigated in this study include temperature condition index (TCI), NDVI deviation (DevNDVI), vegetation condition index (VCI), and vegetation health index (VHI). The drought indices obtained from each satellite image were compared to crop yield data and a selected in-situ-based drought indicator (SPEI) to meet the study's goal. According to the results, the VHI outperformed other drought indices in both satellite images, having the best association with crop yieldand SPEI, followed by DevNDVI, then the VCI, and finally the TCI. In both satellite images, the VHI was found as a suitable index for agricultural drought characterization among the four indices analyzed. VHI is followed by Dev_{NDVI}*, VCI, and TCI. Furthermore, as compared to MODIS images with a coarser geographical resolution, all drought indicators produced from Landsat data with a medium spatial resolution show a stronger connection with crop yield and SPEI. As a result, Landsat data is a useful satellite image for describing agricultural dryness in the research region, and VHI is the appropriate drought index. Accordingly, the agricultural drought situation in the research region throughout the study period was analyzed. According to the findings, drought affected most of the research areas in the years 2000, 2011, 2012, 2015, and 2016. However, during 2006, 2013, and 2018, the study region had near-normal and normal vegetation conditions. Hence, agricultural drought characterization and mapping can be used to guide decision-making processes in drought monitoring and to reduce the adverse effects of the drought on agriculture and the economy.*

Keywords: Agriculture, drought indices, drought monitoring, Landsat, MODIS.

CHAPTER ONE

1. INTRODUCTION

1.1 Background

Drought is a slowly encroaching disaster that mainly occurs due to a reduction in seasonal precipitation below the normal or long-term average (Mishra and Singh, 2010). Drought varieties are grouped into four groups by viewing drought as a hazard: agricultural, meteorological, socio-economical and hydrological droughts (Mishra and Singh, 2010). In most semiarid areas of Ethiopia, including the Tigray Region, where the study area is located, drought caused crop failure and a reduction in agricultural output, which resulted in extended famines and food shortages in the last four decades (Alemu and Yoseph, 2004; Gebrehiwot et al., 2011; Weldearegay and Tedla, 2018; Chere, 2019). Thus, accurate monitoring of drought is necessary to mitigate the adverse effects of the drought on agriculture and the economy.

Monitoring of drought conditions are significantly dependent on the information received regarding drought characteristics, all of which is largely based on the drought indices. Drought indices are a single number used in drought monitoring to define drought features for example spatial extent, duration, and severity by combining data from different indicators such as temperature, precipitation, soil moisture, vegetation condition, stream flow, groundwater, evapotranspiration, and so on (Amalo et al., 2017; Qamer et al., 2019; Zargar, 2011). In Ethiopia, including the study area, agricultural drought monitoring has usually been carried out using the ground based indices, which are calculated from ground measurements of hydro-climatic variables available from meteorological stations (Asheber, 2010; Chere, 2019). In-situ-based drought indices can accurately predict agricultural drought conditions near meteorological stations. However, their ability to monitor and characterize drought conditions at large scale is limited by the absence of continuous geographic coverage of meteorological stations, especially in regions with sparse meteorological stations or high degrees of spatial variability (Hazaymeh and Hassan, 2016; Sun et al., 2020).

Satellite based indices provide a valuable alternative to in-situ-based drought indices since they permit agricultural drought monitoring on a large scale, especially in regions where there is no dense network of station and harsh environmental condition (Hazaymeh and Hassan, 2016).

According to Amalo et al. (2017), Satellite based indices detects, quantifies, and maps drought status in a particular area using satellite data. Recently, several remote sensing-based indices had proposed for different regions, each having a variety of data input requirements and providing different measures of drought (Dalezios et al., 2017; Hazaymeh and Hassan, 2016; Zargar, 2011). However, their limited utility in different regions, and their different assumptions and data input requirements make it necessary to evaluate and validate their suitability for drought characterization in specific regions (Eshetie et al., 2016; Huang et al., 2018; Zhang et al., 2017; Zhuo et al., 2016). In addition, indices derived from different remotely sensed imagery such as moderate resolution imaging Spectro-radiometer, Sentinel, and Landsat have been applied for drought characterization. However, the results of indices derived from different satellite images but for the same target may vary due to the difference in sensor characteristics such as spatial resolution (Al-Bakri et al., 2018; Ke et al., 2015; Psomiadis et al., 2017). Therefore, this study aims to evaluate and compare the performance of four remote sensing-based drought indices for agricultural drought characterization using MODIS and Landsat satellite images in the Tigray Region. This study focused on agricultural drought, which results in a decline in agricultural yield due to (i) short-term precipitation shortages that reduce soil moisture levels and/or (ii) temperature increases that cause an increase in evapotranspiration levels above water supply (Hazaymeh and Hassan, 2016; Panu and Sharma, 2002).

1.2 Statement of the problem

Agricultural drought in the form of crop failure and reduction of agricultural output has been common in the Tigray Region (Alemu and Yoseph, 2004; Chere, 2019; Gebrehiwot et al., 2011). In this regard, accurate and timely information and mitigation of drought would have greater significance in attaining sustainable growth in agricultural productivity and improving the livelihoods of the drought-prone communities. The primary issue in developing advanced drought management and a mitigation policy is the selection of appropriate drought index for accurate and precise drought monitoring and forecasting.

In the study area, in-situ-based drought indices application has been primarily employed for identifying and characterizing agricultural drought (Asheber, 2010; Chere, 2019). Theses indices are based on the point-based weather data collected at the meteorological stations and provide accurate data for drought monitoring around the metrological stations (Hazaymeh and Hassan, 2016; Sun et al., 2020). The irregular spatial dissemination of the meteorological stations over the landscape, however, often imposes uncertainty in defining spatial context. Interpolation of meteorological observations from neighboring stations is often utilized in data-scarce regions like Ethiopia, where there isn't a dense network of stations, resulting in considerable uncertainty about its applicability for drought characterization (Berhan et al., 2011; Hazaymeh and Hassan, 2016; Sun et al., 2020). In contrast, Satellite based indices can provide quick, cost-effective, and spatially continuous information for drought characterization over large geographic areas, particularly in areas with low station density and harsh environmental conditions (Hazaymeh and Hassan, 2016). However, various remotely sensed indices have limited utility in different regions because they are initially developed to characterize drought in particular regions (Bandyopadhyay and Saha, 2016; Huang et al., 2018; Rhee et al., 2010; Zhang et al., 2017; Zhang and Jia., 2013). Moreover, due to the different assumptions and data input requirements of the indices, there is absence of universal index suitable for drought characterization in a specific area (Bandyopadhyay and Saha, 2016; Huang et al., 2018; Sun et al., 2020; Zhuo et al., 2016). Furthermore, the index derived from data obtained over the same target but with different sensors may not be the same due to the difference in sensor characteristics such as spatial resolution (Al-Bakri et al., 2018; Ke et al., 2015; Psomiadis et al., 2017). Since the performance of remote sensing-based drought indices varies among regions and sensor characteristics, performance evaluation and comparison of remote sensing-based drought indices from different sensors is necessary to aid in agricultural drought monitoring. So far, no significant efforts have been made to evaluate the performance of remote sensing-based drought indices in the study area. Thus, the present study is the first attempt to evaluate and compare the performance of four remote sensing-based drought indices for agricultural drought characterization using MODIS and Landsat satellite images in the Tigray Region.

1.3 Objective of the study

1.3.1 General objective

The general objective of this study is to evaluate the performance of four remote sensing-based drought indices for agricultural drought characterization using Landsat and MODIS satellite images.

1.3.2 Specific objectives

The specific objectives are:

- To assess the effectiveness of four indices from Landsat and MODIS images;
- To investigate the suitable satellite image for agricultural drought characterization; and
- To assess the condition of agricultural drought using the best remote sensing-based drought index using a suitable satellite image in the study area.

1.4 Research Questions

The research questions, which the thesis aims to address, include:

- Which index is suitable for agricultural drought characterization from MODIS images?
- Which index is suitable for agricultural drought characterization from Landsat images?
- Which satellite image is suitable for agricultural drought characterization?
- What was the condition of agricultural drought in the study area throughout the study period?

1.5 Significance of the Thesis

Identifying suitable drought index for a specific area is crucial for preparing and mitigating for drought-related disasters. This work may be utilized to improve regional drought monitoring by enabling precise identification of drought conditions, which is required for efficient communication and coordination of drought response or mitigation measures. The result will be crucial in acquisition of better information on the effectiveness of each indicator obtained from various satellite images in agricultural drought characterization. In addition, this will be essential to understand drought events better and differentiation between each index when they are implemented for a particular application and region. Thus, decision-makers will be able to respond to drought-related losses in a timely and effective manner.

1.6 The scope of the Thesis

This study has spatial, temporal, and methodological scopes. Geographically, the scope of the study is focused on the Tigray Region. Methodologically, the study evaluated and compared the four indices using Landsat and MODIS images. Temporally, the study is also limited to 12 years.

1.7 Limitations of the Thesis

Since the required length of data for this kind of study could not be obtained from a single Landsat sensor, this study used diverse sensors (i.e., TM, ETM+, and OLI) equipped with different Landsat platforms (i.e., Landsat 5, 7, and 8), having some different sensor characteristics, but those sensors have the same spatial resolution. Thus, this limited the present study comparing the effectiveness of the MODIS-based indices with the Landsat-based indices only based on their difference in spatial resolution. Thus, other sensor characteristics were not considered in this study.

1.8 Organization of the Thesis

The study was ordered into six chapters, which are stated as follows. Chapter one encompasses the introduction of the study. Chapter two deals with a scientific literature review relevant to the study. Chapter three consists of study area description and a thorough explanation of the methodologies employed for data collection and analysis. The results, discussion, and justification are presented in the fourth and fifth chapters based on the findings of the research output. Finally, chapter six consists of the conclusion and recommendations of the study.

CHAPTER TWO

2. LITERATURE REVIEW

2.1 Concept and Types of Drought

Drought is a climatic event that occurs when seasonal precipitation, runoff, and soil moisture drop below normal or long-term average (Mera, 2018; Mishra and Singh, 2010; Qamer et al., 2019). Areas with dry climates are more frequently affected by drought because of a reduction in soil moisture and seasonal rainfall variability (Qamer et al., 2019). Drought is a climatic disaster with a significant impact on the society, agriculture, environment, and the economy. By considering drought as a hazard, drought types are grouped into four main categories: hydrological, meteorological, socio-economic and agricultural drought (Mishra and Singh, 2010). A meteorological drought is mostly caused by a shortage of precipitation compared to average conditions over a specific location and period. In addition, high evaporation, low humidity, desiccating winds, and increased temperatures are considered factors for the occurrence of meteorological drought (Hazaymeh and Hassan, 2016). Contrary to this, deficiency in surface runoff, stream flow, reservoir, or groundwater level caused hydrological drought (Legesse and Suryabhagavan, 2014). On the other hand, agricultural drought is the reduction in soil moisture availability below the optimal level required for the proper growth of plants during critical periods of the growth cycle that results from some of the effects of meteorological and hydrological drought (Hazaymeh and Hassan, 2016; Qamer et al., 2019). Finally, socioeconomic drought incorporates features or impacts of hydrological, agricultural, and meteorological droughts (Hazaymeh and Hassan, 2016).

2.2 Causes of Drought

With increasing temperatures, evapotranspiration, and rainfall variability, climate change is projected to have serious effects on soil, land cover, and hydrologic systems (Hazaymeh and Hassan, 2016; Panu and Sharma, 2002). In Africa drought phases have a distinct natural component: they are influenced in part by geophysical events that cause the continent's humidity to change.

Soil moisture desiccation, nonlinear climate system behavior, and ENSO are recognized as the possible causes of drought in this region (Haile, 2005; Lyon, 2014; Tierney et al. 2013). In East Africa, the complexity and variability of the El Niño-Southern Oscillation (ENSO) are among the main driving forces of drought (Masih et al., 2014). Temperature and precipitation variations across the world, and seasonal weather in surrounding parts of the equatorial Pacific, are all affected by ENSO episodes. As a result, ENSO are recognized as key influencing factors for drought in Africa (Masih et al., 2014). Beyond the effect of climate variability, anthropogenic effects on the environment have also changed drought patterns under conditions of a growing population (Masih et al., 2014). These effects include land use change, land degradation, deforestation, fire, and mining. Droughts are also influenced by human activities like overuse of water resources, increased settlements and urbanization, and the expansion of agricultural and pasture fields (Zeng, 2003). Generally, in the Sahel area, anthropogenic variables such as land degradation, land use change, firing, deforestation, and mining, and changes in air movement resulting from multi-decadal fluctuations in global sea surface temperature, have all been recognized as the main causes of drought (Dai 2011; Zeng, 2003).

2.3 The Impact of Drought

Due to its slow onset, lengthy duration, cumulative impacts, and widespread over large geographical areas, drought is considered as a complex and strong environmental disasters that results in environmental, social, and economic costs around the world (Kogan, 1997; Tadesse et al., 2004). Droughts are most severe in dry and semi-arid areas, when there is less water available. Drought consequences are also dependent on the sensitivity of a sector or activity, not just the intensity of the hazard. As a result, because agriculture differs geographically, the susceptibility to the same drought and the impact varies. Drought results in several significant impacts (direct and indirect). Direct drought effects include reduced forest, rangeland productivity, cropland, and water levels, increased wildlife and livestock mortality rates. The effects of these direct impacts are considered indirect impacts. Moreover, drought effects may be grouped by the affected sector, leading to environmental, economic, or social types of impact. Specifically, environmental impacts refer to the losses that result as a direct consequence of drought or indirectly, such as wildfire damage to plant and animal species. Similarly, many economic impacts affect agriculture and related sectors.

Finally, social impacts refer to public safety, health, quality of life issues, water-use conflicts, and regional inequities in relief and impact distribution.

2.4 Drought in Ethiopia

Historically, many of the drought-induced food emergencies in the world have occurred in Africa. According to Minamiguchi (2005), 57 percent of the world's drought events recorded by the Centre for Research on the Epidemiology of Disasters in the EM-DAT have occurred in Africa. However, all areas within Africa are not equally vulnerable to drought. The sub-Saharan part of the region is considered to be the most drought-prone. This region is relatively drier, receiving much lower rainfall compared with the rest of the region. Ethiopia is one of the sub-Saharan African countries highly prone to drought. Ethiopia has experienced a number of severe droughts. For instance, in the past century, there were about 30 major drought episodes. 13 of these drought periods are known to have affected the entire country and were classified as severe (Gebrehiwot et al., 2011). Among the natural disasters that occurred in Ethiopia, drought was the country’s major hazard over the past three decades (Asheber, 2010; Gebrehiwot and Van Der Veen, 2013). According to Mera (2018), drought in Ethiopia affected particularly all sectors, including water resources, hydropower (inadequate water for industry and reduced electricity production), and agriculture (loss of livestock and crops), which resulted in population migration, malnutrition, famine, disease and a chain of consequences for farm families.

Tigray is one of the regions of Ethiopia affected by a repeated cycle of drought and food security problems. Populations engaged in agriculture are particularly at risk from drought as agriculture is the major climate-sensitive economic activity. Drought has frequently affected crop and livestock production in most parts of Tigray. Over the years, farmers have experienced the worst effects of drought in terms of their loss of crop yield and livestock, and sometimes crop failure due to scarcity of water during peak growth stages of the crop. The magnitude of this is well understood by the fact that the region is an agricultural region, with 82% of the population directly dependent on agriculture for their livelihood. Due to the abnormalities in terms of both spatial and temporal distribution of precipitation, drought is a frequent phenomenon which causes instability in food production over many parts of the region.

Table 2.1 Major drought years, areas affected and effects in Ethiopia during 1965–2015. (Source: https://public.emdat.be/data)

Year	Location	Associated
1965	Nationwide	
1973	Tigre, Wollo, North Shoa, Tigray, Kangra provinces	Famine
1983	Wollo, Gondar, Goe, Eritrea, Tigrai, Shoa, Harerge, Sidamo	
1987	Ogaden, Eritrea, Tigray, Wello, Shewa, Gama, Gofa, Sidamo, Gondar, Bale	
1989	Northern Ethiopia, Eritrea, Tigray, Wollo, Gondar, Harerge	Food shortage
1997	Borena, Bale (Oromiya state) South Ome zone, Somali state	
1999	North Wollo, South Wollo, Oromia, Wag Himra districts (Amhara province), Southern district (Tigray province), Beneshangul Gumu, Gambela, Oromia, SNNPR, Somali provinces	Food shortage
2003	Tigray, Oromia, Amhara, Somali, Afar provinces	
2005	Afder, Liben districts (Somali province), Gode zones (Shabelle district, Somali province), Borena district (Oromiya province)	Food shortage
2008	Oromia, Somali, Amhara, Afar, Tigray, SNNPR provinces	Famine
2009	Somali, Oromia, Afar, Tigray, Amhara, SNNP, Gambela provinces	Food shortage
2010	Somali, Oromia, Afar, Tigray, Amhara provinces	
2011	Dire Dawa, Gambela, Hareri, Oromia, SNNPR, Somali, Addis Ababa provinces (Southern Ethiopia)	Food shortage
2015	Somali, Afar, Oromia, Amhara	Famine

Figure 2.1 Crop failure due to drought in Ethiopia.

(source:https://www.open.edu/openlearncreate/mod/oucontent/view.php?id=79970&section=5)

Figure 2.2 Children in the study area are collecting maize grains that dropped from trucks loaded with relief food (Photo by Dechassa Lemessa, UN-EUE, February, 2003).

Figure 2.3 Photo showing crop failure due to recurring drought event in the study area (source: Asheber, 2010).

2.5 Drought Monitoring and Assessment Approaches

The immediate and more devastating impact of drought is on agricultural crops, leading to reduction of production, unemployment, food shortages, etc. Thus, there is a need for effective monitoring of agricultural drought, its onset, progression, and impact on crops to minimize the damage. Drought monitoring is a continuous analysis process that includes numerous indicators of drought severity using drought indices, and the impact and spatial extent. It is one of the three key steps in drought risk management programs, along with drought preparedness and drought response. Agricultural drought monitoring entails measuring and assessing different agro-climate variables in agricultural areas in order to develop appropriate agricultural drought evaluation indicators. These assessments are subsequently interpreted into drought reports that objectively and accurately identify the characteristics of drought conditions. Usually, such combined information can be used in early warning systems prior to drought occurrences.

Timely and accurate information on potential drought episodes would have greater significance in reducing regional disasters and agricultural losses. Drought monitoring is usually implemented with indicators and/or indices. Drought indices are a single number used in drought monitoring to define the characteristics of drought such as spatial extent, severity, duration, and by integrating data from one or several variables such as temperature, precipitation, vegetation condition, soil moisture, stream flow, groundwater, evapotranspiration, etc. (Amalo et al., 2017; Qamer et al., 2019). Indices are important elements for drought detection, monitoring, forecasting, and assessment, as they summarize complex interrelationships between multiple climate parameters in a way that is more readily understandable for decision-making. Agricultural drought monitoring is usually done using indices. According to Hazaymeh and Hassan (2016), based on the data and technology used, agricultural drought indices can be categorized into in-situ based and satellite based (remote sensing based) agricultural drought indices.

2.6 In-situ Based Agricultural Drought Indices

The in-situ indices are based on one or more ground readings of climatic variables such as rainfall, stream flow, groundwater, evapotranspiration, temperature, relative humidity, or other variables available from climatic, agricultural, and hydrologic stations (Qamer et al., 2019). These indices can provide the longest-term and most accurate quantitative and qualitative information related to agricultural drought conditions at the point locations where the input data are collected. However, to approximate the values of the indices between weather stations and achieve a continuous spatial coverage of data, interpolation must be utilized. Spatial interpolation often leads to uncertainties (Hazaymeh and Hassan, 2016; Sun et al., 2020). Recently, most of these problems have been tackled by using satellite data that provides a permanent data archive, cost effectiveness, and a regular, repetitive view of nearly all of the earth's surfaces (Zhang et al., 2017). Some of the most commonly used in-situ based agricultural droughts monitoring indices are summarized in Table 2.2.

2.6.1 Remote sensing-based Agricultural Drought Indices

Satellite based indices use products from satellite sensors to assess the drought condition of the area (Hazaymeh and Hassan, 2016). Satellite data is a more quick, cost-effective, and powerful tool for drought monitoring than using observational data (Amalo et al., 2017). Satellite (remote sensing) based indices are based on the distinct spectral signatures of soil surface and canopy features, especially in the red, near infrared, shortwave infrared and thermal spectral bands. Hazaymeh and Hassan (2016) states that, the development of these indices for drought characterization depends on the idea that drought can influence the chemical and bio-physical properties of vegetation and soil, such as vegetation biomass, chlorophyll content and soil moisture etc. Most of these indices rely on the difference between the absorption of radiation in the visible red spectral domain (which vegetation absorbs) and the reflectance in the near infrared (which vegetation strongly reflects) electromagnetic spectrum. Normalized Difference Vegetation Index (NDVI) was developed by Tucker (1979), and is used to evaluate the health and density of vegetation by measuring the difference between near-infrared and red light. Most of the satellite instruments measure the NIR and red bands, which makes NDVI easy to calculate by using various data sources. The other advantage of NDVI is that the NDVI algorithms (i.e., the use of "ratio") help in cancelling out a significant amount of signal variation linked to calibration or change in the irradiance conditions resulting from various meteorological phenomena such as sun angle or shadow cast by clouds (Qamer et al., 2019).

Table 2.2: Most commonly used in-situ based agricultural drought monitoring indices.

Index	**Inputs**	**Advantage**	**Disadvantage**	**Source**
Crop Moisture Index (CMI)	Precipitation and temperature	Easley calculated using temperature and precipitation data	Not suitable for long-term assessment of agricultural drought	Palmer, 1968
Crop Specific Drought Index (CSDI)	Temperature, precipitation, evapotranspiration	Estimates the availability of soil water for different zones and soil types on a daily basis.	Too many data input requirements including, climatological data, crop phenology, and soil type.	Meyer et al., 1991
Evapotranspiration Deficit Index (ETDI)	Weekly evapotranspiration and soil moisture values	In its calculations, it takes into account the water stress ratio and provides weekly values that reflect short-term dry situations.	Due to increased evapotranspiration and irregular precipitation, the spatial variation of its values increases throughout the summer season.	Narasimhan and Srinivasan, 2005
Palmer Drought Severity Index (PSDI)	Temperature, precipitation, soil moisture, evapotranspiration	Provides a more comprehensive understanding of the drought situation.	sophisticated computation.	Palmer, 1965
Soil Moisture Drought Index (SMDI)	Weekly evapotranspiration and soil moisture values	Improves the ability for modeling and monitoring hydrologic system and soil moisture deficient at a finer resolution	Irrespective to soil properties across different climatic conditions	Narasimhan and Srinivasan, 2005
Standardized Precipitation Index (SPI)	Precipitation	Simple to use, simply requires precipitation data, and measures drought conditions on various time frames.	Only use precipitation, which is difficult to interpolate across huge areas.	Mckee et al., 1993
Standardized Precipitation Evapotranspiration Index (SPEI)	Temperature and precipitation	Overcome the shortcomings of precipitation drought index such as SPI in addressing the consequences of climate change on drought behavior.	SPEI is virtually identical to SPI or other precipitation drought indexes when there are no apparent temporal changes in temperature.	Vicente et al., 2010

NDVI deviation (DEV_{NDVI}) can identify the severity of drought conditions by comparing the current NDVI value of an area with the long-term mean of the same time. When the DEV_{NDVI} is negative, it indicates below-normal vegetation conditions and might suggest a drought situation (Tucker, 1979). It's effectively monitored agricultural drought conditions in different studies (Bandyopadhyay and Saha, 2016; Berhan et al., 2011; Gedif et al., 2014; Thenkabail et al., 2004; Eshetie et al., 2016; Melese, 2016). In 1990, Kogan (1990) introduced an index, which is based on long-term NDVI values and called the vegetation condition index (VCI). The VCI is stated in % and indicates where the measured value falls in relation to the prior year's extreme values (minimum and maximum). A low value of VCI would be an indication of stressed vegetation due to unfavorable weather conditions, while a high value of VCI indicates healthy vegetation conditions. VCI has been used in many agricultural drought-monitoring studies (Gebrehiwot et al., 2011; Liou and Mulualem, 2019). It was also used in conjunction with other indices like DEVNDVI (Bandyopadhyay & Saha, 2016; Gedif et al., 2014; Thenkabail et al., 2004; Eshetie et al., 2016; Melese, 2016). Moreover, Land Surface Temperature, which is derived from thermal channels of various satellite instruments, can provide use full information in assessing evapotranspiration, soil moisture and vegetation condition (Qamer et al., 2019). The effectiveness of land surface temperature was used as a base line for the development of indices based on the thermal infrared spectrum, such as the Temperature condition index (TCI). Kogan (1995) developed an index called TCI that uses thermal data to determine stress on vegetation caused by temperature and excessive wetness. In TCI, drought conditions are estimated relative to the minimum and maximum land surface temperatures (Kogan, 1995). The minimum land surface temperature in an area is indicative of the presence of moisture in the soil and thus relative vegetation or crop health, while the maximum land surface temperature indicates the thermal stress that leads to water deficit conditions and consequent vegetation or crop stress. Low TCI values (near to 0%) suggest that the month or week will be extremely hot. Low TCI values continue over time, which could signify the start of a drought (Kogan, 1995). TCI can provide use full information in drought due to thermal effects and identify subtle changes in vegetation health due to high temperatures accompanied by moisture shortages. TCI outperformed NDVI and VCI, according to Kogan (1995) and Qamer et al. (2019), notably in conditions of high soil moisture induced by severe rainfall or continuous cloudiness. Indeed, these circumstances can cause low VCI and NDVI values, which might be misinterpreted as drought.

Table 2.3Most commonly used remote sensing based drought monitoring indices

Index	**Expression**	**Advantage**	**Disadvantage**	**source**
Normalized Difference Vegetation Index	NDVI = $\frac{NIR-R}{NIR+R}$	Provides a measure of vegetation health or greenness conditions	Sensitive to darker and wet soil conditions; also demonstrates time lag in response to soil moisture	Tucker, 1979
Vegetation Condition Index	$VCI = (\frac{NDVI_i - NDVI_{min}}{NDVI_{max} - NDVI_{min}})$	Provides vegetation greenness conditions	Data from a longer time period is required.	Kogan, 1990
Moisture Stress Index	$MSI = (\frac{SWIR}{NIR})$	More sensitive at canopy level rather than leaf level	Applicable for densely vegetated areas	Hunt and Rock, 1989
Normalized Difference Water Index	NDWI = $(\frac{NIR - SWIR}{NIR + SWIR})$	Effective in monitoring water content in vegetation	In the presence of soil and poorly vegetated or bare surfaces, uncertainty increased significantly.	Gao, 1996
Temperature condition index	$\mathrm{TCI} = (\frac{\mathrm{LST_{max}} - \mathrm{LST_i}}{\mathrm{LST_{max}} - \mathrm{LST_{min}}}) * 100$	Easy to get the required input data	Requires clear-sky conditions at the time of imaging	Kogan, 1995
TRMM Precipitation Condition Index	$PCI = (\frac{TRMM - TRMM_{min}}{TRMM_{max} - TRMM_{min}})$	Works well at regional size under most weather circumstances.	Low spatial resolution and inability to gather images at higher latitudes.	Zhang and Jia, 2013
Normalized Moisture Inde	$NMI = NDVI + NDWI$	Combines both vegetation greenness and wetness conditions.	Not recommended for short-term drought assessment	Jang et al., 2006
Vegetation health index	$\mathrm{VHI} = 0.5 * \mathrm{VCI} + (1 - 0.5) * \mathrm{TCI}$	Provides more comprehensive drought monitoring capabilities	Requires appropriate data fusion for VCI and TCI	Kogan, 1997
Temperature -vegetation index	$TVX = \frac{LST}{NDVI}$	Depicts drought conditions at regional scale	TVX/VSWI slopes may vary from one place to another	Lambin and Ehrlich, 1996

Furthermore, because different indices have diverse capabilities in monitoring and detecting agricultural drought, researchers have tried to combine them into unified drought indices in the aim of better characterizing drought situations. Vegetation Health Index (VHI) was developed by Kogan (1997) as a function of temperature condition index and Vegetation condition Index. The VHI is also an effective tool because it incorporates the VCI, calculated from normalized difference vegetation index values, which indicates the impact of moisture on vegetation, while the TCI, which is a function of the LST, indicates the impact of temperature on vegetation. The VHI was found as a sensitive index for detecting and quantifying agricultural drought (Amalo et al., 2017; Arekhi et al., 2020; Brema et al., 2019; Ghaleb et al., 2015; Zhuo et al., 2016). Some of the most commonly used remote sensing based agricultural droughts monitoring indices are summarized in Table 2.3.

2.7 Drought Monitoring in Ethiopia

Assessing and analyzing drought is crucial in water resource management and planning. Drought conditions are assessed under socio-economic, meteorological, hydrological and agricultural aspects. Drought assessment depends on the factors that caused the drought. Assessing drought requires the understanding of historical droughts and its impact during the drought (Qamer et al., 2019). In Ethiopia including the study area, drought assessments usually done in conventional method (ground data collection and analysis) to identify drought -prone areas performed manually by the taskforce from government, NGO and UN agencies by DPPC as a leading organization of the team (Gedif et al., 2014). Because of the low density of weather stations, the traditional approach to drought monitoring and early-warning systems that involves ground-based data collection is laborious, time-consuming, and challenging (Legesse and Suryabhagavan, 2014). Aside from that, data isn't available in a rapid enough manner to allow for somewhat accurate and timely large-scale drought identification and monitoring. This leads to inaccurate result in assessment of drought. Policy makers and non-governmental organization cannot accurately target the area which need help the most and result in poor targeting. This makes difficult to prioritize drought mitigation based on the risk level.

The detection, monitoring and mitigation of disasters require gathering of rapid and continuous relevant information that are not effectively collected by conventional methods. Satellite tools and techniques allow for the quick acquisition and distribution of continuous information over broad regions. A satellite circumnavigating the earth can survey the entire surface in a few days and repeat the survey at regular intervals, but an aircraft can only survey a small region at a time. Drought monitoring based on satellite can offer continuous and frequent information on the surface characteristics of planar surfaces while taking full advantage of surface spectrum information. It can provide drought monitoring that is both macro and dynamic. Drought monitoring over wide areas may now be done via satellite.

2.8 Evaluation of the Performance of Drought Indices

Drought assessment is important in the management and planning of water resources. Some standard is necessary for assessment so that drought parameters can be compared across regions and with previous drought episodes (Heim, 2002; Wable et al., 2018; Zargar et al., 2011). For this, more than 150 drought indices have been developed for this purpose, and new indices are being developed based on new technology for estimating drought consequences, each with its own set of advantages and drawbacks. Different studies show that many drought indices have limited utility because they are often developed to monitor drought for a specific region and application under specific hydro-climatic conditions (Heim, 2002; Wable et al., 2018; Zargar et al., 2011). Due to the complex nature of drought phenomena and differences in hydro-climatic conditions, there isn't a uniform drought index for analyzing drought conditions in different parts of the world. Accordingly, performance evaluation of various drought indices is necessary to find a suitable drought index for a specific application in a specific region (Eshetie et al., 2016; Huang et al., 2018; Heim, 2002; Quiring and Papakryiakou 2003; Wable et al., 2018). And also, evaluation of the performance of drought indices helps to understand drought events better and allows differentiation between each index when they are implemented for a particular application (Heim, 2002; Wable et al., 2018; Zargar et al., 2011).

For more than three decades, with the development of remote sensing technology, several remote sensing-based agricultural drought indices for agricultural drought monitoring have been proposed for different places, having a variety of data input requirements and providing different measures of drought. Despite the continued development and improvement of remotely sensed drought indices, the accurate assessment of drought remains difficult. The challenge in applying remote sensing-based drought indices in drought monitoring and in issuing early warnings is that the various indices have limited utility under different hydro-climatic conditions because they are often developed to monitor drought in specific regions. Several researchers across the world have compared different remote sensing-based agricultural drought indices with the aim of finding suitable drought indexes for agricultural drought monitoring in specific regions, such as Amalo et al. (2017) in East Java, Eshetie et al. (2016) in East Amhara, Sun et al. (2020), Huang et al. (2018) and Zhuo et al. (2016) in Northern China. Even though many studies have compared drought indices, the results have confirmed that their performance varies with the application and region of interest. This is due to the spatial and temporal occurrence and severity of agricultural drought differing from one region to another in accordance with the climate and hydrology of the area (Bandyopadhyay & Saha, 2016; Eshetie et al., 2016; Huang et al., 2018; Rhee et al., 2010). Due to the different assumptions and data input requirements of remotely sensed drought indices, there is a lack of a universal remote sensing based drought index suitable for assessing agricultural drought conditions (Bandyopadhyay & Saha, 2016; Huang et al., 2018; Sun et al., 2020; Zhuo et al., 2016).

In addition, remote sensing-based agricultural drought indices derived from different satellite data such as moderate resolution imaging spectro-radiometer (MODIS), Landsat, Sentinel, and AVHRR have been widely used for agricultural drought assessment. However, due to the various sensor characteristics such as spatial resolutions and instrument performances, there are differences between remote sensing based agricultural drought indices derived from multiple sensors for the same target (Al-Bakri et al., 2018; Huang et al., 2020; Ke et al., 2015; Psomiadis et al., 2017). Accordingly, different researchers recommend examining the effectiveness of different remote sensing-based drought indices before applying them to a particular application in a specific region.

2.9 Approaches for Evaluating the Performance of Drought Indices for Agricultural Drought Monitoring

Several studies evaluate the performance of different drought indices for agricultural drought monitoring. Generally, those studies used one or two of the three methods, which include: i) performance evaluation by examining their ability to characterize historical drought events; ii) performance evaluation by comparing them with in-situ based agricultural drought indices; and iii) performance evaluation by investigating their relationship with crop yield data.

In the first technique, the performance of drought indices for agricultural drought monitoring is evaluated by comparing drought features generated from the drought index with the corresponding characteristics of the recorded historical drought occurrences in the area. This method is useful for determining the distinction between and ability of each drought index to characterize the severity, frequency, and persistence of drought events (Morid et al., 2006; Wable et al., 2018; Amalo et al., 2017). However, the lack of precise records of drought events makes this approach difficult to apply. In this study, this evaluation method was not used because of the unavailability of recorded data related to the characteristics of major historical drought events.

The second technique is founded on the notion that variations in climatic factors like precipitation and temperature in terms of meteorological drought affect agricultural productivity and are considered the main cause of agricultural drought (Alexandrov and Hoogenboom, 2000). Accordingly, the in-situ indices were mostly used for agricultural drought characterization. According to Hazaymeh and Hassan (2016), the in-situ indices were proposed for monitoring meteorological drought. However, they can provide the longest-term and most accurate information related to agricultural drought near metrological stations. Therefore, the performance of satellite indices for drought characterization can be evaluated by comparing with the in-situ indices at the point locations where the input variables are acquired (Shad et al., 2017; Sun et al., 2020; Thenkabail et al., 2004).

The third technique is founded on the notion that crop yield loss is a clear indicator of the direct effects of agricultural drought (Huang et al., 2018).Accordingly, different researchers, such as Huang et al. (2018); Leon et al. (2019); Thenkabail et al. (2004);

Tian et al. (2018); Todisco et al. (2008); and Zhuo et al. (2016), confirmed that the performance of indices can be evaluated by comparing with crop yield data. Due to the lack of data from major historical drought events, the two final methods were chosen for evaluating the performance of remote sensing-based drought indices for agricultural drought characterization in this study.

2.10 Empirical Review on the Performance Evaluation of Remote Sensing Based Drought Indices for Agricultural Drought Monitoring

Previous studies, such as Zhang and Jia (2013); Zhang et al. (2017); and Rhee et al. (2010), evaluated the effectiveness of remote sensing-based drought indices in different climatic regions. Their finding demonstrates that the performance of remote sensing-based drought indices varies with the region of interest. Moreover, Huang et al. (2018), Shad et al. (2017), and Zhuo et al. (2016) showed the performance difference of remote sensing-based drought indices in irrigated and rain-fed regions. Furthermore, Al-Bakri et al. (2018) and Ke et al. (2015) indicated that the performance of remote sensing-based drought indices for drought assessment varies due to the difference in sensor characteristics such as spatial resolution and instrument performance. As the performance of remote sensing-based drought indices varies among regions and sensor characteristics, several studies have been conducted to find suitable drought indices for agricultural drought monitoring in specific regions.

For instance, Al-Bakri et al. (2018) compare different indices (Normalized Difference Vegetation Index (NDVI), moisture stress index (MSI), evapotranspiration water stress indicator (EWSI), perpendicular drought index (PDI), and modified perpendicular drought index (MPDI) derived from MODIS for assessing drought conditions in the Mafraq area in Jordan. Also, the possible improvement in drought monitoring as a result of improved spatial resolution is also investigated in this study by comparing Landsat-based indices with MODIS-based indices. The finding showed the Landsat-based indices with medium spatial resolution were better at detecting agricultural drought conditions than MODIS-based indices with coarser spatial resolution. Also, PDI was shown to be the most accurate indicator that was highly correlated with soil moisture measurements. Similar to this finding, other studies also found that remote sensing-based drought indices derived from finer spatial resolution images perform better and are more sensitive when used to investigate agricultural drought (Al-Bakri et al., 2018; Arekhi et al., 2020; Brema et al., 2019; Hazaymeh and Hassan, 2016; Siburian, 2018).

A study conducted by Eshetie et al. (2016) evaluates the performance of four remote sensing-based drought indices (actual evapotranspiration anomaly (Eta), Vegetation Condition Index (VCI), Normalized Difference Vegetation Index (NDVI), and NDVI deviation (Dev_{NDVI})) for agricultural drought monitoring in East Amhara, Ethiopia. The performance evaluation was carried out by analyzing the relationship between drought indices and crop yield data. The result of the study shows that Dev_{NDVI} has more capability to monitor agriculture droughts than VCI and NDVI, which are slightly higher than those of the Eta. Therefore, for operational applications, Dev_{NDVI} was recommended by the study for agricultural drought monitoring and early warning in East Amhara. Similarly, prior studies indicated DevNDVI had better performance than VCI for agricultural drought monitoring in semi-arid areas (Bandyopadhyay and Saha, 2016; Melese, 2016).

Moreover, a study by Zhuo et al. (2016) compares the performance of the temperature condition index (TCI), vegetation condition index (VCI), vegetation health index (VHI), temperature vegetation dryness index (TVDI) and drought severity index (DSI) for agricultural drought monitoring in irrigated and rain-fed regions of China. The study evaluates the performance of the indices by comparing their relationships with crop yield data. Based on the study, the TVDI outperformed the five drought indices, followed by DSI, VHI, VCI, and TCI. Also, the remote sensing-based indices performed better in the rain-fed region. Furthermore, Huang et al. (2018) assessed the effectiveness of the vegetation health index (VHI), temperature vegetation dryness index (TVDI) and drought severity index (DSI) for monitoring agricultural drought in two major agricultural production regions in Shaanxi and Henan provinces, northern China (predominantly rain-fed and irrigated agriculture, respectively). The study compared the remote sensing based indices with the in-situ based drought index, crop yield, and soil moisture data. The study finds that DSI outperformed the other indices, with stronger correlations with SPI, soil moisture, and crop yield data. In addition, the remote sensing-based indices have better agreement with SPI, soil moisture, and crop yield data in Shaanxi (predominantly rain-fed agriculture) than in Henan provinces (predominantly irrigated agriculture). Finally, the study concludes that remote-sensing-based agricultural drought indices provide more accurate predictions of the impacts of drought in predominantly rain-fed agricultural areas.

Furthermore, Sun et al. (2020) proposed a new remote sensing based drought index called the Vegetation Drought Monitor Synthesized Index (VDSI) by integrating three remote sensing based drought indices, namely the Standardized Vegetation Index (SVI), the Standardized Water Index (SWI) and the Evaporative Stress Index (ESI) in the northeast China. Then the study compared the performance of the new remote sensing-based drought index (VDSI) with the three single remote sensing-based indices (ESI, SVI, and SWI). Crop yield data and an in-situ based drought index were used to evaluate the performance of the indices. Accordingly, VDSI performed better for agricultural drought monitoring than the three single remote sensing-based indices (ESI, SVI, and SWI). Finally, the study concluded that agricultural drought monitoring could be aided by combining data from several indicators.

CHAPTER THREE

3. MATERIALS AND METHODS

3.1 Description of the study area

The study area, Tigray, is one of the regional states of Ethiopia located in the northern part of the country. Geographically, it lies between latitudes 12° 15' and 14° 57'N and longitudes 36° 27' and 39° 59'E, covering a total area of 5,260,600 Ha (Figure 3.1) (Gebrehiwot et al., 2011). The study area is bordered by Sudan to the west, Eritrea to the north, the Amhara Region to the south, and the Afar Region to the east and southeast.

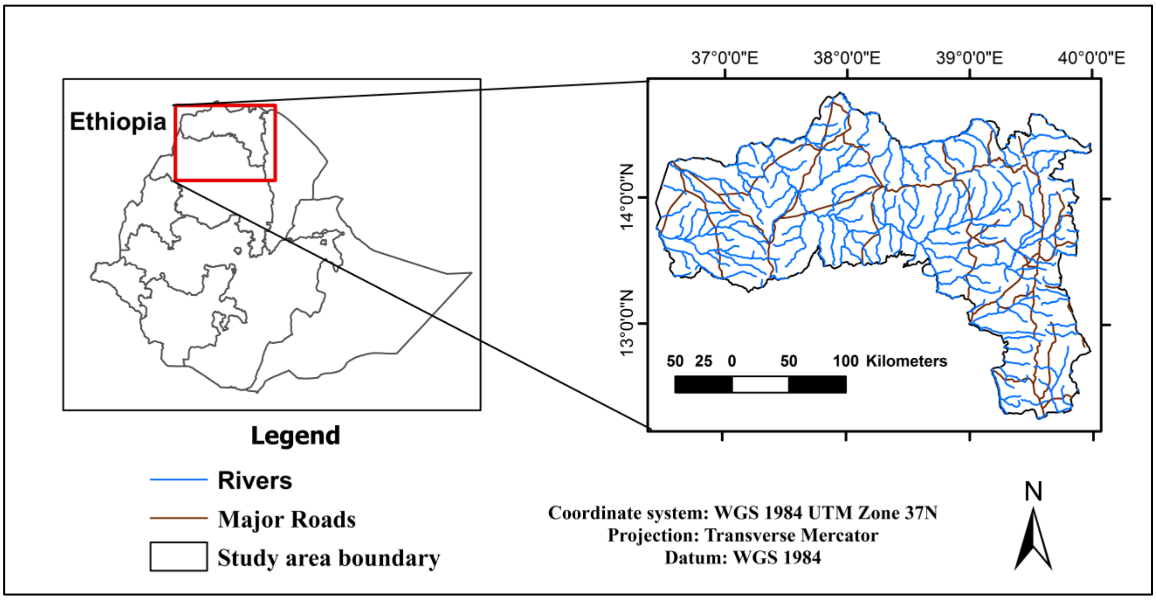

Figure 3.1 Location map of the study area

Tigray Region has a total population of 4,316,988 with an average family size of five peoples per household (CSA, 2008). From the total population, 844,040 (19.5%) and 3,472,948 (80.5%) were urban and rural residents, respectively. According to CSA (2008), the population is growing at a rate of 2.5 percent per year and population density in the region is 86.6 persons per square kilometer, showing a high population pressure.

Like the rest of Ethiopia, the economy of Tigray is heavily dependent on low productivity rain-fed agriculture that strongly dependent on timely onset amount and distribution of rainfall (Asheber, 2010; Gebrehiwot et al., 2011). Agriculture is the main source of the economy for the majority of the population. It covers about 57% of gross domestic product (GDP), of which 36% is from crop production and about 17% and 4% are from livestock and forestry, respectively (Asheber, 2010). Crop husbandry, animal husbandry and mixed farming are the main farming systems, of which mixed farming is the dominant type of farming system. Smallholder agriculture predominates, with an average land holding of less than one hectare per family (Gebrehiwot et al., 2011; Gebrehiwot and Van Der Veen, 2013). Smallholder farmers manage crop and animal production in an integrated way, to maximize returns from their limited land and capital, minimize production risk, diversify sources of income, provide food security and increase productivity. Agricultural systems in the region are characterized by traditional technology based entirely on animal pull and rain-fed agriculture. Almost all of the cropland is planted to annual food crops, including cereals (teff, wheat, barley, maize, sorghum, millet), pulses (beans, chick peas, lentils), and oilseeds (sesame, flax). According to CSA (2018), cereals (teff, wheat, maize and sorghum) are the major food crops in terms of area planted and volume of production in the region. Because of the frequent drought, food shortages are the central challenge in the region (Asheber, 2010).

Climatically, the region belongs to the sub-tropical climate, which is characterized by the sparse and highly uneven distribution of seasonal rainfall and frequent drought (Tefera et al., 2019). From a climatic standpoint, there are three distinct seasons: the dry winter season, which runs from October to February; the hot pre-monsoon season, which runs from March to May; and the rainy monsoon season, which runs from June to September (locally known as "kiremt"), during which 80 percent of the crops are cultivated (Gebrehiwot et al., 2011). The region has a rainfall peak in July and August and minimum rainfall between December and February (Figure 3.3). Climatically, the average monthly temperature of the region varies between 16.4 °C and 21.6 °C (Figure 3.2). The minimum average temperature was recorded in December and the maximum average temperature was recorded in May.

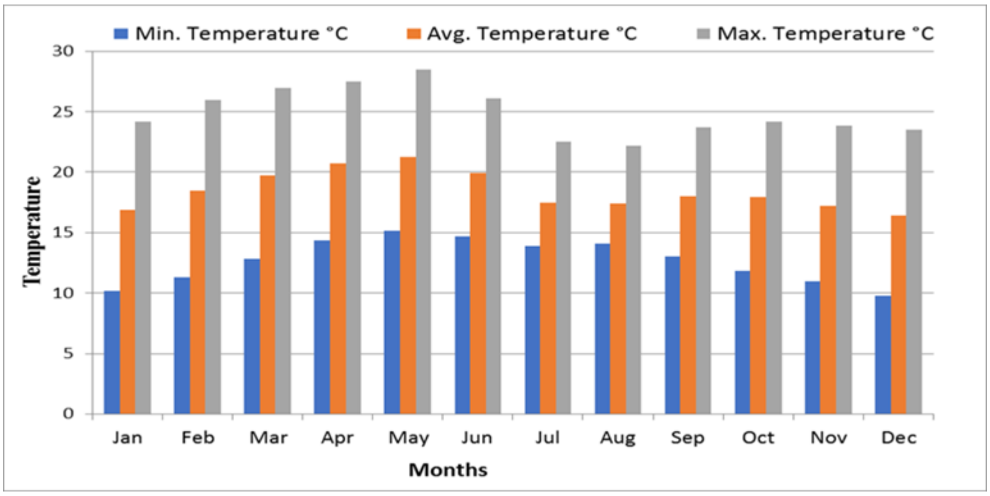

Figure 3.2: Monthly temperature variation during 2000 - 2018.

(Source: National Meteorological Agency of Ethiopia)

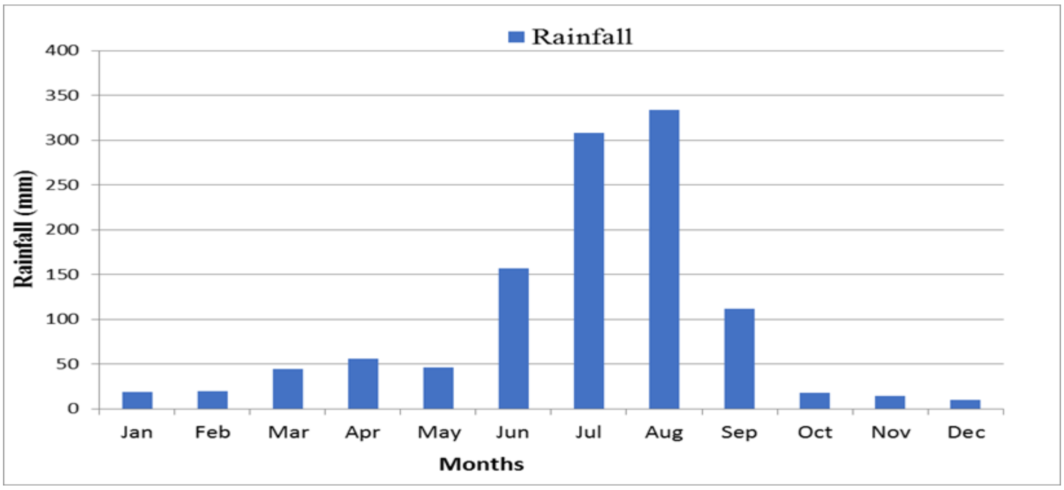

Figure 3.3: Average monthly rainfall distribution between 2000 and 2018.

(Source: National Meteorological Agency of Ethiopia)

3.2 Data

The source, acquisition period and spatial resolution of the data used in this study were summarized in Table 3-1.

Table 3.1: Data type and sources

Data set	**Spatial resolution (m)**	**Period**	**Source**	**Purpose**
Landsat 7 (ETM+)	30	2005 to 2008 and 2011 to 2012	USGS	
Landsat 8(OLI/TIRS)	30	2013 to 2016 and 2018	USGS	For calculating drought indices from Landsat image
Landsat 4-5 (TM)	30	2000	USGS	
MOD13Q1 NDVI	250	2000, 2005 to 2008, 2011 to 2016 and 2018	USGS	For calculating drought indices from MODIS image
MOD11A2 LST	1000	2000, 2005 to 2008, 2011 to 2016 and 2018	USGS	
Meteorological Data	-	1989-2018	NMA	For SPEI calculation
Crop Yield data	Quintal/H	2000-2018	CSA	For performance evaluation of drought indices
Tigray Region boundary	-		GII	To extract the study area

3.2.1 Remote sensing data

The Landsat (TM, ETM+, and OLI) and MODIS (MOD13Q1 NDVI and MOD11A2 LST and Emissivity) images were downloaded from the Earth Explorer Website operated by the USGS (https://earthexplorer.usgs.gov/). The Landsat (TM, ETM+, and OLI) images with 168/50, 168/51, 169/50, 169/51, 170/50, and 170/51 (path/row) were downloaded at a 30 m spatial resolution, while the MOD13Q1 NDVI and MOD11A2 LST and Emissivity images had a spatial resolution of 250 and 1000 m, respectively. The MODIS and Landsat images were used to calculate the remote sensing-based agricultural drought indices from MODIS and Landsat images, respectively. With the exception of the years 2001 to 2004, 2009, 2010, and 2017, when the cloud-free Landsat images were not available, both satellite images were gathered during the maximum growing season of agricultural crops (September) in the research area from 2000 to 2018. Because cloud cover frequently influenced Landsat satellite imagery during the early phases of the growing season, the maximum growing season was chosen for this study. According to Arekhi et al. (2020); Brema et al. (2019) and Al-Bakri et al. (2018), because crop performance during the maximum growing season is one of the indicators of agricultural drought, assessing the crop's status during the maximum growing season is an essential aspect that should be considered in agricultural drought monitoring studies of high and medium resolution data.

According to Gidey et al. (2018a) and Owrangi et al. (2011), ten years of satellite observation data were required to conduct this kind of study. Thus, in this study, twelve years of data were considered in both Landsat and MODIS satellite images.

3.2.2 Meteorological data

Rainfall and temperature data from 38 stations for the period of 1989 to 2018 were collected from the National Meteorological Agency (NMA) of Ethiopia (Appendix B). The names and locations of weather stations are summarized in Appendix B. The rainfall and temperature data were used to compute the in-situ based drought index called the Standardized Precipitation Evapotranspiration Index (SPEI). SPEI was used to evaluate the performance of remote sensing-based drought indices.

3.2.3 Crop yield data and Crop calendar

The crop yield data for the major cereals of the study area from 2000 to 2018 was obtained from the Central Statistical Agency (CSA) (Appendix A). The crop yield data was used to assess the effectiveness of remote sensing-based drought indices. In addition, the crop calendar was used to select the maximum growing season of crops in the study area. According to CSA (2018), cereals (teff, wheat, maize, and sorghum) are the major food crops in terms of area planted and volume of production in the study area. Accordingly, the crop calendar of the main cereals in the study area was obtained from the Group on Earth Observations Global Agricultural Monitoring Initiative (GEOGLAM) at the regional level. According to GEOGLAM (2019), the crop-growing season in the study area is between May to October, while the maximum growing season is in September (Table 3.2). In addition to the GEOGLAM crop calendar, prior studies in the study area verified that the Meher crop growing season for cereals was from May/June to September/October (Chere, 2019; Eze et al., 2020; Gebrehiwot et al., 2011).

Table 3.2: Crop calendar of major cereals in Tigray Region (GEOGLAM, 2019).

Crop type									
Teff									
Sorghum									
Wheat									
Maize									
	May	Jun	Jul	Aug	Sep	Oct	Nov	Dec	Jan
	Planting			Growing			Harvesting		

3.3 Software packages

Table 3.3 Software packages used

Software name	Purpose
ArcGIS	For drought indices calculation
Microsoft Excel	For data analysis and generation of graphs and charts
SPSS	For statistical analysis and graphical display
R studio	For SPEI calculation
Hydrognomon	For double mass curve analysis
QGIS	For image pre-processing

3.4 Methodology

The methodology adopted for this study is shown in a flow chart in Figure 3.4. The performance evaluation of remote sensing-based drought indices using Landsat and MODIS images comprises the following major steps: Initially, the Landsat satellite image has been examined for preprocessing requirements, which include atmospheric and radiometric correction, cloud masking, and extraction of the research area. In addition, the MODIS imagery was re-projected, clipped by the shape file of the study area, and poor quality MODIS data was masked out. Subsequently, the Landsat and MODIS images were used to compute the remote sensing-based drought indices from Landsat and MODIS images, respectively. Moreover, the quality of rainfall and temperature data were checked and used to calculate the in-situ based drought index (SPEI). Furthermore, the performance evaluation of the indices from both satellite images was done by assessing their agreement with SPEI and crop yield. Finally, the research region's agricultural drought status was examined using the best remote sensing based agricultural drought index from an appropriate sensor. The steps of the methodology have been briefly described in the subsequent sub-sections.

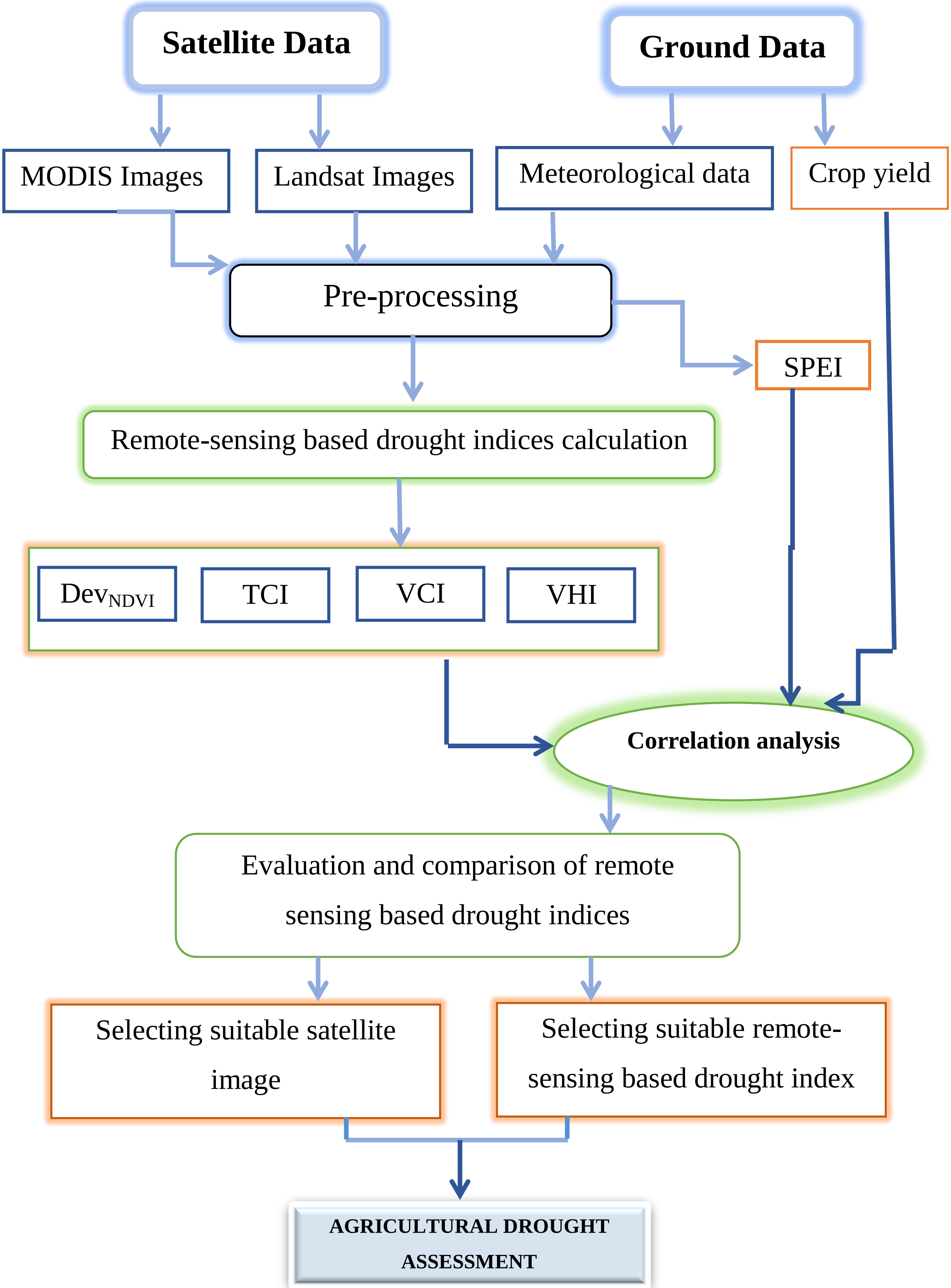

Figure 3.4: Methdological flow chart

3.5 Data Processing and analysis

3.5.1 Image Preprocessing

Since the acquired Landsat data is subject to distortion caused by sensor, solar, and atmospheric effects, image preprocessing are necessary to improve the quality of the image data, which is helpful for further analysis. Landsat 7 ETM+ images acquired after 2003 had striping problem due to the failure of the scan-line corrector (SLC) in 2003. The striping problems were corrected by using the linear interpolation technique. In addition, the Landsat images passed through a number of subsequent preprocessing techniques, including cloud masking, mosaicking, and extraction of the research region. Furthermore, the following processing, such as radiometric and atmospheric corrections, was made to the Landsat image to increase the data quality.

Geometric correction: The processing levels of the collected Landsat TM, ETM+ and OLI images were L1T (Level 1 Terrain Corrected) which were already geometrically corrected with sufficient accuracy using ground control points and the digital elevation model as well (USGS, 2015). Therefore, there is no need for geometric correction for this data.

Radiometric correction and calibration: According to Chander et al. (2009), radiometric calibration is the process of converting DN to spectral radiance and then to top of the atmosphere (TOA) reflectance to minimize errors in the digital numbers of images. The detail radiometric correction process, including conversion to at-sensor spectral radiance, conversion to top of atmosphere (TOA) reflectance and Conversion to top of atmosphere brightness in Landsat images were summarized in (Appendix C).

Atmospheric correction: Atmospheric correction is needed to remove the atmospheric effect on the scene, which is necessary for accurate retrieval of land surface reflectance values. Different atmospheric correction methods were developed, such as Dark Object Subtraction (DOS), Fast Line-of-Sight Atmospheric Analysis of Spectral Hypercubes (FLAASH), and Quick Atmospheric Correction (QUAC). According to Zhang et al. (2010) and Dewi and Trisakti (2017), Dark Object Subtraction is better than other methods for removing atmospheric effects from Landsat imageries. Thus, the Dark Object Subtraction (DOS 1) atmospheric correction method in QGIS was used to produce a surface reflectance value (Chavez, 1996).

According to Didan et al. (2015) and Wan (2006), the MOD13Q1 NDVI and MOD11A2 LST and emissivity images were already corrected for molecular scattering, ozone absorption, and aerosols. Thus, the MOD13Q1 and MOD11A2 LST data for the study area were masked out, re-projected from sinusoidal projection to the Universal Transverse Mercator projection (UTM, Zone 37) WGS84 projection, and poor quality MODIS data was masked out. Moreover, the 1 km of MOD11A2 LST and emissivity data were resampled to 250 m to be consistent with MOD13Q1 NDVI data.

3.5.2 Computation of Remote Sensing-based Drought Indices from MODIS and Landsat Imageries

Normalized Difference Vegetation Index (NDVI): NDVI computed from Landsat and MODIS images was used as an input to compute the VCI and DEV_{NDVI} from Landsat and MODIS images, respectively. The surface reflectance value of the red and near-infrared bands (bands 3 and 4) of TM and ETM+ and (bands 4 and 5) of Landsat 8 OLI/TIRS was used to calculate NDVI from TM, ETM+, and OLI/TIRS as follows (Tucker, 1979):

$$NDVI = \frac{(NIR-R)}{(NIR+R)} \tag{1}$$

To calculate NDVI from the MODIS image, the extracted MOD13Q1values were rescaled with a scale factor of 0.0001 (Didan et al., 2015). According to Ganie and Nusrath (2016), the value of NDVI ranges from -1 to +1, in which NDVI less than zero shows a water body, the NDVI range between 0 and 0.1 shows bare soil, and NDVI greater than 0.1 indicates vegetation. Accordingly, the NDVI values below 0.1 have been reclassified in all datasets as they represent areas other than vegetation (Chere, 2019; Eshetie et al., 2016). As a result, the remote sensing-based drought indices from each sensor were computed using NDVI values larger than 0.1.

Land Surface Temperature (LST): the LST computed from Landsat and MODIS images was used as an input to compute the temperature condition index from Landsat and MODIS images, respectively.

To calculate LST from MODIS sensor, the extracted MOD11A2 LST data were rescaled to obtain the correct LST, and converted to degree Celsius (°C) units as follows (Wan, 2006):

$$\mathrm{LST} = (\omega * 0.02) - 273.15 \tag{2}$$

where LST is Land Surface Temperature in Degree Celsius, ω is Row Scientific data (SDS).

The computation of land surface temperature from Landsat data was continued by using the calculated brightness temperature obtained after radiometric correction in Appendix C. Landsat 7 ETM+ includes the thermal band in low-gain (6L) and high-gain (6H). In this study, the radiance measured by the ETM+ 6H (high gain) thermal band was used because of its higher radiometric precision than the 6L (low gain) (Chander et al., 2009). In addition, the high-gain (6H) thermal band of ETM+ is more accurate for obtaining temperature information than the low-gain band due to its closeness to the real field conditions (Coll et al., 2010). On the other hand, the Landsat 8 OLI/TIRS is equipped with a thermal-infrared band for bands 10 and 11. However, the United States Geological Survey (USGS) has notified the use of only Band 10 data of Landsat 8 OLI/TIRS due to the larger calibration uncertainty associated with Band 11 data of Landsat 8 OLI/TIRS caused by stray light effects (USGS, 2019). Due to that, band 10 data from Landsat 8 OLI/TIRS was used to compute LST from Landsat 8.

The brightness temperature values obtained in Appendix C were calculated by considering the earth's surface as a black body. However, the ground is not a black body. Thus, the ground emissivity has to be considered for computing the thermal radiance emitted from the ground. Therefore, corrections for spectral emissivity (e) became necessary. The land surface emissivity (LSE) was computed from NDVI using the formula by Sobrino et al. (2004):

$$\varepsilon = 0.004 * P_V + 0.986 \tag{3}$$

Where:

ε – Land surface emissivity

P_V - Proportion of vegetation, and was calculated by the formula (Sobrino et al., 2004):

$$P_V = \left[\frac{NDVI - NDVI_{min}}{NDVI_{max} - NDVI_{min}}\right]^2 \tag{4}$$

Finally, the emissivity corrected land surface temperatures from Landsat TM, ETM+, and OLI/TIRS sensors were computed as follows **(**Artis and Carnahan, 1982, Macarof et al., 2018, Nwilo et al., 2019):

$$LST = \frac{T_B}{1+(\lambda \times T_B/\rho)ln\varepsilon} \qquad (5)$$

Where LST is Land Surface Temperature in Celsius; TB is Brightness Temperature; λ is Wavelength of the emitted radiance (11.5 μm); ε is land surface emissivity and ρ = 1.438 ×10-2 mk (constant).

3.5.2.1 NDVI Deviation (Dev_{NDVI})

The NDVI deviation (Dev_{NDVI}) from each image was computed by using the NDVI value calculated from each image as follows (Tucker, 1979):

$$\text{DevNDVI} = NDVI_i - NDVI_{mean} \qquad (6)$$

Where $NDVI_i$ is the NDVI value for the year i and $NDVI_{mean}$ is the long term average of NDVI.

3.5.2.2 Vegetation Condition Index (VCI)

NDVI obtained from each images were used to compute vegetation Condition Index (VCI) as follows (Kogan, 1990):

$$VCI = \left(\frac{NDVI_i - NDVI_{min}}{NDVI_{max} - NDVI_{min}}\right) * 100 \qquad (7)$$

Where $NDVI_i$ is the current NDVI value, $NDVI_{min}$ and $NDVI_{max}$ are a multi-year minimum and maximum NDVI.

3.5.2.3 Temperature Condition Index (TCI)

The TCI from each satellite image was computed using the LST generated from each image as an input. The TCI was computed using the following equation (Kogan, 1995):

$$\text{TCI} = \left(\frac{\text{LST}_{\text{max}} - \text{LST}_{\text{i}}}{\text{LST}_{\text{max}} - \text{LST}_{\text{min}}}\right) * 100 \qquad (8)$$

Where LST_i is the current LST value, LST_{max} and LST_{min} are the multi-year maximum and minimum LST.

3.5.2.4 Vegetation Health Index (VHI)

The TCI and VCI computed from Landsat and MODIS images were used as an input to compute the VHI from Landsat and MODIS images, respectively. VHI was computed using the formula (Kogan, 1997):

$$\mathrm{VHI} = \mathrm{a} * \mathrm{VCI} + (1 - \mathrm{a}) * \mathrm{TCI} \qquad (9)$$

Where VHI is Vegetation Health Index, a is 0.5 (contribution of VCI and TCI) and VCI is Vegetation Condition Index, TCI is Temperature Condition Index.

In the VHI calculation, an equal weight has been assumed for both VCI and TCI, since temperature and moisture contribution during the vegetation cycle are currently unknown (Kogan, 2001). The lower VHI value (≤ 40) indicated that the high incidence of agricultural drought whereas a higher VHI value (> 40) show wet or non-drought conditions Table 3.4 (Kogan, 2001; Bhuiyan et al., 2017).

Table 3.4: drought class classification based on VHI value (Bhuiyan et al., 2017; Kogan, 2001).

Drought category	**Values**
Extreme	<10
Severe	<20
Moderate	<30
Mild	<40
No	≥40

3.5.3 Preprocessing of Meteorological Data

In order to use the rainfall and temperature data obtained from the ground station, the quality of the meteorological data was checked. The weather data obtained from stations in the study area was found to have certain data gaps and a shortage of record length. In this study, based on Hosking and Wallis (2005), stations having more than 20% of missing monthly data were discarded from use. Accordingly, 16 stations having less than 20% of missing data were selected, and missing data was estimated by using the normal ratio (NR) method. This method mainly depends on the mean ratio of climate data between neighboring stations and the target station in order to weigh the impact of each neighboring station. According to Armanuos et al. (2020), the NR method provides the most accurate estimate of climate data in Ethiopia, including the study area. In addition, the double mass curve technique was applied to check and adjust the consistency and homogeneity of climate data in the selected station with the help of Hydrognomon software. The double mass curve produced for each station (Appendix D) demonstrates the consistency of the climate data.

3.5.4 Standardized Precipitation and Evapotranspiration Index (SPEI)

Vicente et al. (2010) developed the SPEI as a meteorological drought index or as an in-situ based agricultural drought index based on precipitation and temperature data, and it has the advantage of combining a multi-scalar character with the ability to include the effects of temperature variability in drought assessment. According to Vicente et al. (2010), a minimum of 30 years of data should be used to calculate the index. In this multi-scale index, potential evapotranspiration (PET) is subtracted from the precipitation. According to Stagge et al. (2014), the potential evapotranspiration (PET) value can be calculated using a different range of equation types, including temperature-based, radiation-based, and combination equations. According to Vicente et al. (2010), the estimated SPEI does not vary significantly with the PET method used, but occasionally some methods, in general, provide better results for PET quantification than others. In dry and semi-arid environments, however, Beguería et al. (2014) found significant differences in SPEI computed using different PET methodologies. Beguería et al. (2014) proposed Penman-Monteith as the best option for the estimation of PET for the calculation of SPEI, followed by the Hargreaves and Thornthwaite methods. However, the Penman-Monteith method requires sunshine, humidity, and wind speed data along with temperature data, which are all spatially and temporally inadequate in the study area. The Thornthwaite method only requires the mean daily temperature and a suitable method for the calculation of PET in data-scarce regions such as Ethiopia. Therefore, the simplest approach to calculate PET, which is the Thornthwaite method (Thornthwaite, 1948) was used in this study. The temperature and rainfall data from 1989 to 2018 were used to calculate SPEI using the R Studio SPEI package. The detailed calculations of PET and SPEI are summarized in Appendix E.

Earlier studies showed that vegetation does not immediately respond to climatic factors such as precipitation and temperature (Gebrehiwot et al., 2011; Workie and Debella, 2018). According to Workie and Debella (2018), there was a one-month time lag between vegetation and climatic factors in the study area.

Thus, by considering a one-month lag between vegetation and meteorological factors, the three-month SPEI at the end of August was calculated at 16 meteorological stations and used to evaluate the performance of remote sensing-based drought indices. According to Delbiso et al. (2017); Temam et al. (2019) and Teweldebirhan et al. (2019), this time scale (i.e., three months) is better to capture the drought events affecting agriculture. The three-month SPEI calculated in August compares the total difference in precipitation and PET (P-PET) from June to August of that specific year to the total difference in precipitation and PET (P-PET) from June to August of all the years studied (30 years).

3.5.5 Performance Evaluation of Remote Sensing-Based Drought Indices

3.5.5.1 Remote Sensing-based Drought Indices *vs.* Crop yield

The direct impact of agricultural drought can be clearly shown by a reduction in crop yield (Huang et al., 2018; Quiring and Papakryiakou, 2003). Accordingly, different researchers, such as Huang et al. (2018); Leon et al. (2019); Tian et al. (2018); Todisco et al. (2008); Zhuo et al. (2016); Thenkabail et al. (2004), confirmed that the performance of the remote sensing-based drought index for agricultural drought monitoring can be evaluated by comparing their agreement with crop yield. Thus, the agreement of remote sensing-based indices derived from both satellite images and crop yield was investigated and compared. A correlation analysis was performed between crop yield and the mean raster cell values of drought indices derived from both satellite images.

3.5.5.2 Remote Sensing-based Drought Indices *vs.* In-situ-based Drought Index

According to Hazaymeh and Hassan (2016) and Sun et al. (2020), the in-situ-based drought indices can provide the most accurate information related to agricultural drought conditions at the point locations where the input variables are acquired. Therefore, the performance of remote sensing-based drought indices can be evaluated by comparing their agreement with the in-situ based drought indices at the point locations where the input variables are collected (Arekhi et al., 2020; Huang et al., 2018; Rhee et al., 2010; Shad et al., 2017; Sun et al., 2020; Thenkabail et al., 2004). Therefore, the in-situ-based drought index called the Standardized Precipitation and Evapotranspiration Index (SPEI), which uses the standardized measure of precipitation (P) minus evapotranspiration (PET), was selected to evaluate the performance of remote sensing-based indices. While SPEI is a meteorological drought indicator and does not explicitly model soil moisture dynamics, it is known to correlate well with agricultural droughts as the atmospheric water budget (P-PET) affects surface soil dryness (Vicente et al., 2012; Wang et al., 2014). Moreover, this in-situ-based drought index (i.e., SPEI) had a better performance in agricultural drought monitoring than other in-situ-based indices (Tian et al., 2018; Vicente et al., 2012).

Therefore, the agreement of remote sensing-based indices derived from both satellite images and SPEI was examined and compared. The remote sensing-based indices from both satellite images were extracted at the locations of the meteorological stations, and correlation analyses were performed between the mean raster values of the remote sensing-based indices extracted at the locations of the meteorological stations and the corresponding mean SPEI values of meteorological stations.

The Pearson's Correlation Coefficient (r) was calculated to evaluate the correlation between remote sensing-based indices and SPEI and also between remote sensing-based indices and crop yield. In addition, the Evans (1996) standard (Table 3-5) was adopted to determine the level of strength of the Pearson's Correlation Coefficient (r) between remote sensing-based indices and SPEI and also between remote sensing-based indices and crop yield.

Table 3.5: Strengths of Pearson correlation matrix (Evans, 1996, as cited in Gidey et al., 2018b)

Positive relationship		Negative relationship	
Coefficients (r)	Strength	Coefficients (r)	Strength
≥ 0.60	Strong	≥ -0.60	Strong
0.40 to 0.59	Moderate	-0.40 to -0.59	Moderate
< 0.40	Weak	<- 0.40	Weak

CHAPTER FOUR

4. RESULTS

4.1 MODIS-based Agricultural drought indices *vs.* SPEI

Figure 4.1 shows the relationship between the MODIS-based agricultural drought indices and SPEI. The result revealed a positive and significant correlation between drought indices and SPEI (Figure 4.1). The result indicated that among the remote sensing-based drought indices computed from MODIS sensor, the VHI showed the highest agreement ($r = 0.57$, $P < 0.01$) with SPEI (Figure 4.1 (a)), followed by DevNDVI ($r = 0.5$, $P < 0.05$) (Figure 4-1 (b)) and VCI ($r = 0.44$, $P < 0.05$) (Figure 4.1 (d)). TCI from the MODIS sensor has the lowest correlation with SPEI ($r = 0.4$, $P < 0.05$) (Figure 4.1 (c)).

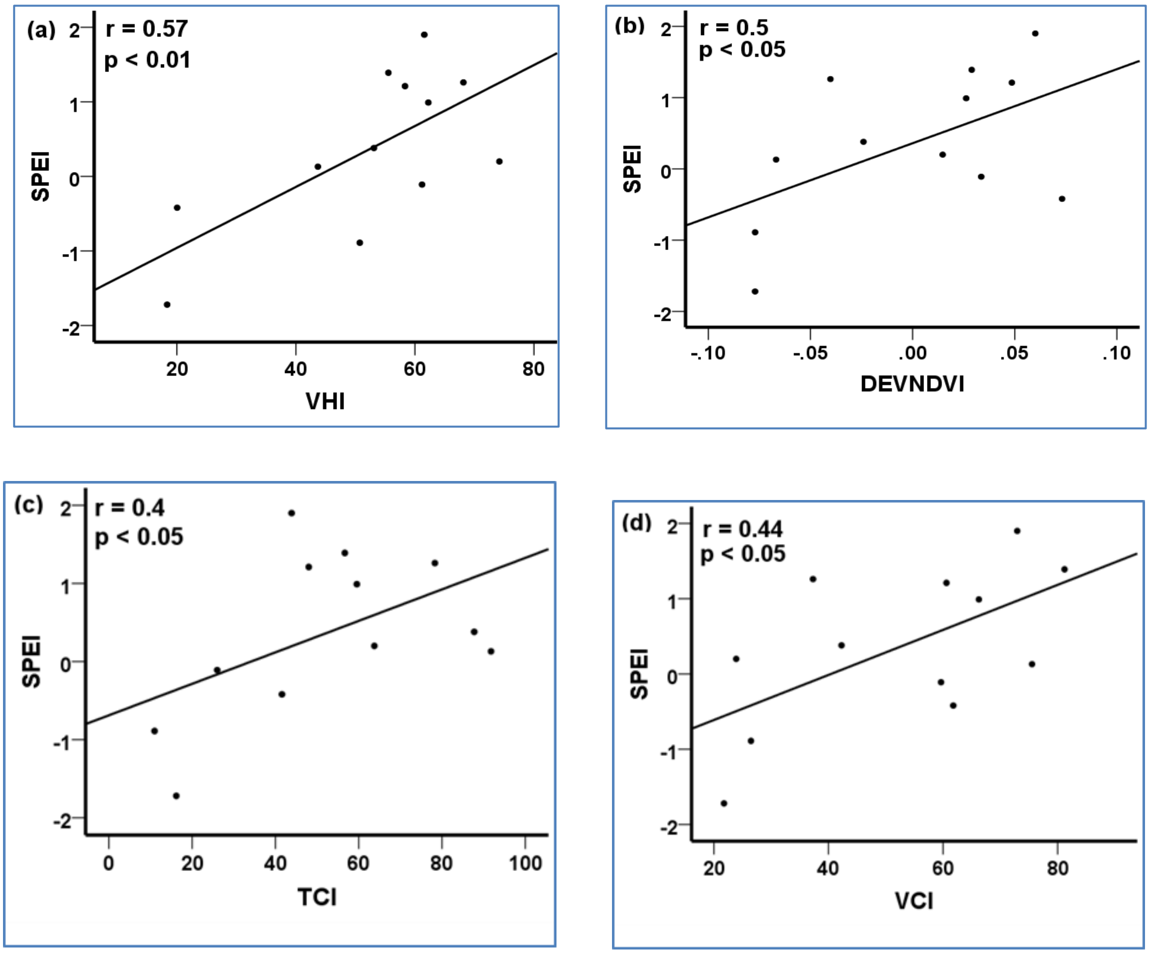

Figure 4.1: Scatter plots showing the relationship between SPEI and MODIS-based agricultural drought indices.

4.2 MODIS-based Agricultural drought indices *vs.* Crop yield

The correlation between MODIS-based agricultural drought indices and crop yield data was illustrated in Figure 4.2. As depicted in the illustrations, the correlation between crop yield and VHI was the highest (r = 0.62, P < 0.01) (Figure 4.2 (a)), followed by DevNDVI (r = 0.54, P < 0.05) (Figure 4.2 (b)), and VCI (r =0.49, P < 0.05) (Figure 4.2 (d)), while it was the lowest with TCI (r = 0.33) (Figure 4.2 (c)).

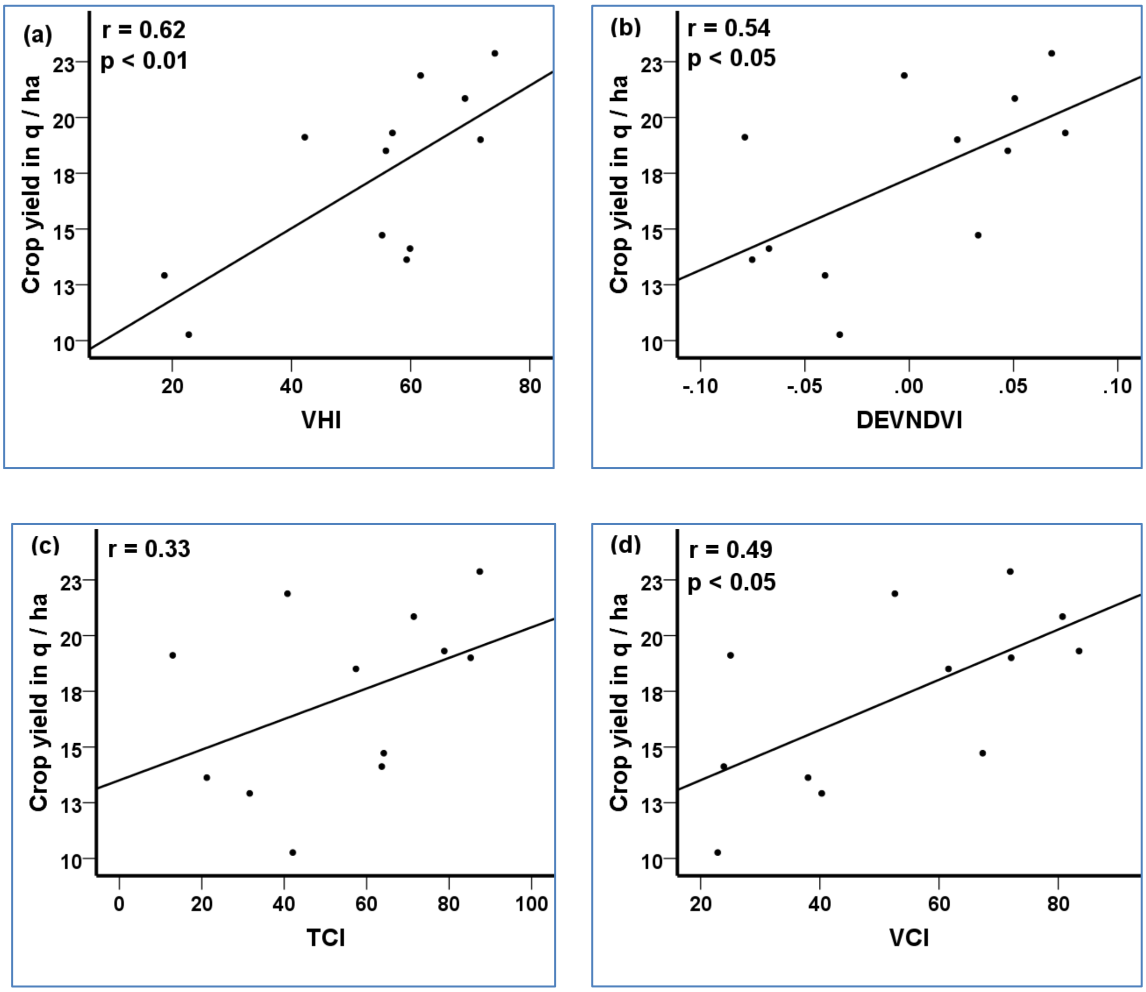

Figure 4.2: Scatter plots showing the relationship between crop yield and MODIS-based agricultural drought indices.

4.3 Identification of Suitable Remote sensing-based Drought Index from MODIS Image

The performance comparison among MODIS-based agricultural drought indices obtained in Sections 4.1.1.1 and 4.1.1.2 is summarized in Table 4.1. It is revealed that the VHI has the highest agreement (r=0.57 and r=0.62, p<0.01) with both SPEI and crop yield respectively, followed by DevNDVI (r=0.5 and r=0.54, p<0.05), and next by VCI (r=0.44 and r=0.49, p<0.05), whereas comparatively, TCI has the lowest correlation (r=0.4, p<0.05 and r=0.33) with both crop yield and SPEI respectively, (Table 4.1).

The overall result indicates that the VHI is the suitable remote sensing-based agricultural drought index from the MODIS sensor for agricultural drought characterization in the study area, followed by Dev_{NDVI} and then VCI, and TCI.

Table 4.1: Performance comparison among MODIS-based agricultural drought indices using Pearson's Correlation Coefficient (r).

Variables	Performance Evaluation using r			
	Dev_{NDVI}	TCI	VCI	VHI
SPEI	0.5*	0.4*	0.44*	**0.57****
Crop yield	0.54*	0.33	0.49*	**0.62****

**. Correlation is significant at the 0.01 level

*. Correlation is significant at the 0.05 level

The highest correlation coefficient values are shown in bold.

4.4 Landsat-based Agricultural drought indices *vs.* SPEI

A positive and substantial relationship was discovered when Landsat-based drought indices were compared to SPEI (Figure 4.3).The result indicates the correlation between SPEI and VHI was the highest (r = 0.63, P < 0.01) (Figure 4.3 (a)), followed by DevNDVI (r=0.55, P< 0.05) (Figure 4.3 (b)) and VCI (r=0.48, P< 0.05) (Figure 4.3 (d)), while TCI exhibited the lowest association (r=0.44, P < 0.05) with SPEI (Figure 4.3 (c)).

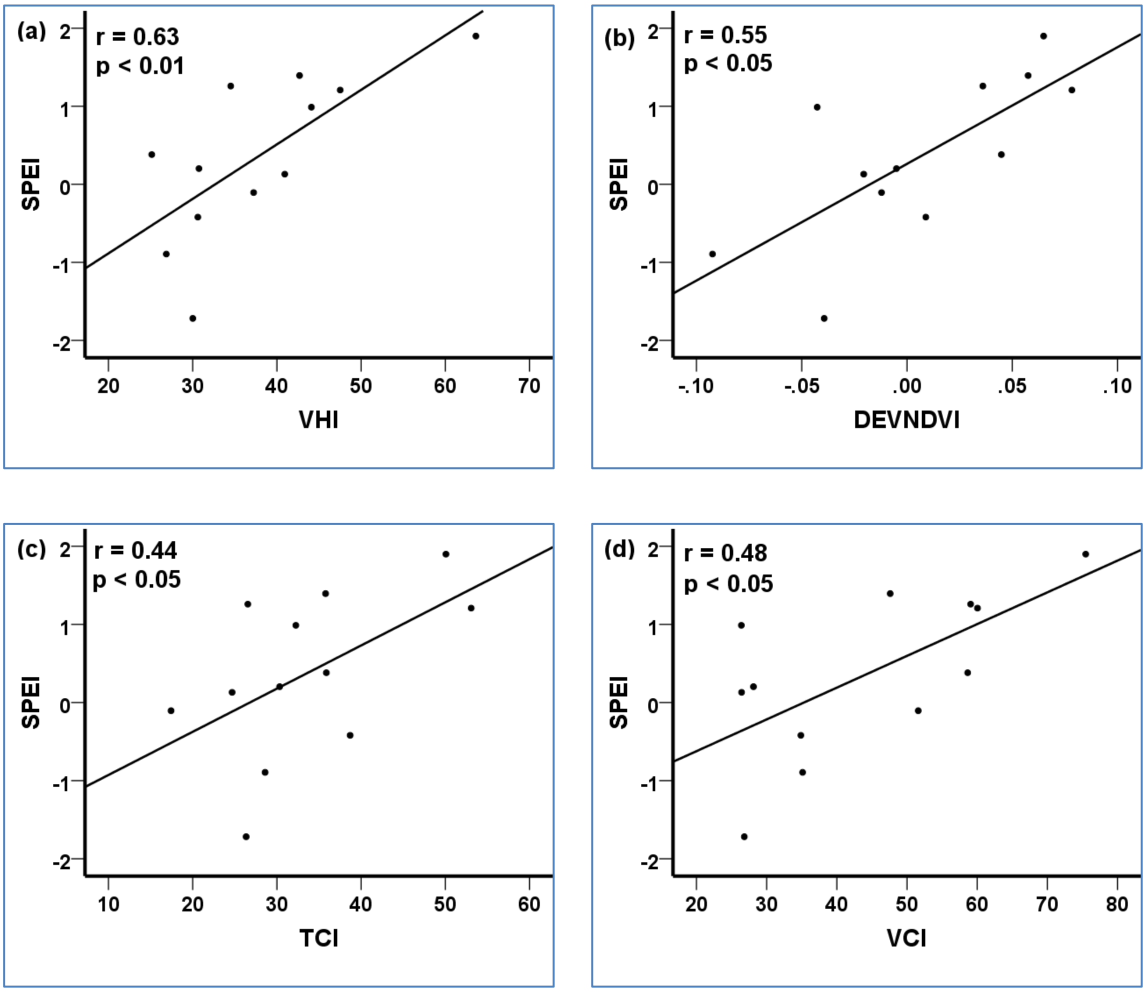

Figure 4.3: Scatter plots showing the relationship between SPEI and Landsat-based agricultural drought indices.

4.5 Landsat-based Agricultural drought indices *vs.* Crop yield

The link between crop yield and Landsat-based agricultural drought indices is seen in Figure 4.4. The association between crop yield and VHI ($r=0.67$, $p<0.01$) was the largest, while the correlation between crop yield and TCI was the lowest ($r=0.4$) (Figure 4.4 (a) and Figure 4.4 (c)). According to the results, DevNDVI ($r=0.59$, $p<0.05$) also beats VCI ($r=0.55$, $p<0.05$) (Figure 4.4 (b) and Figure 4.4 (d)).

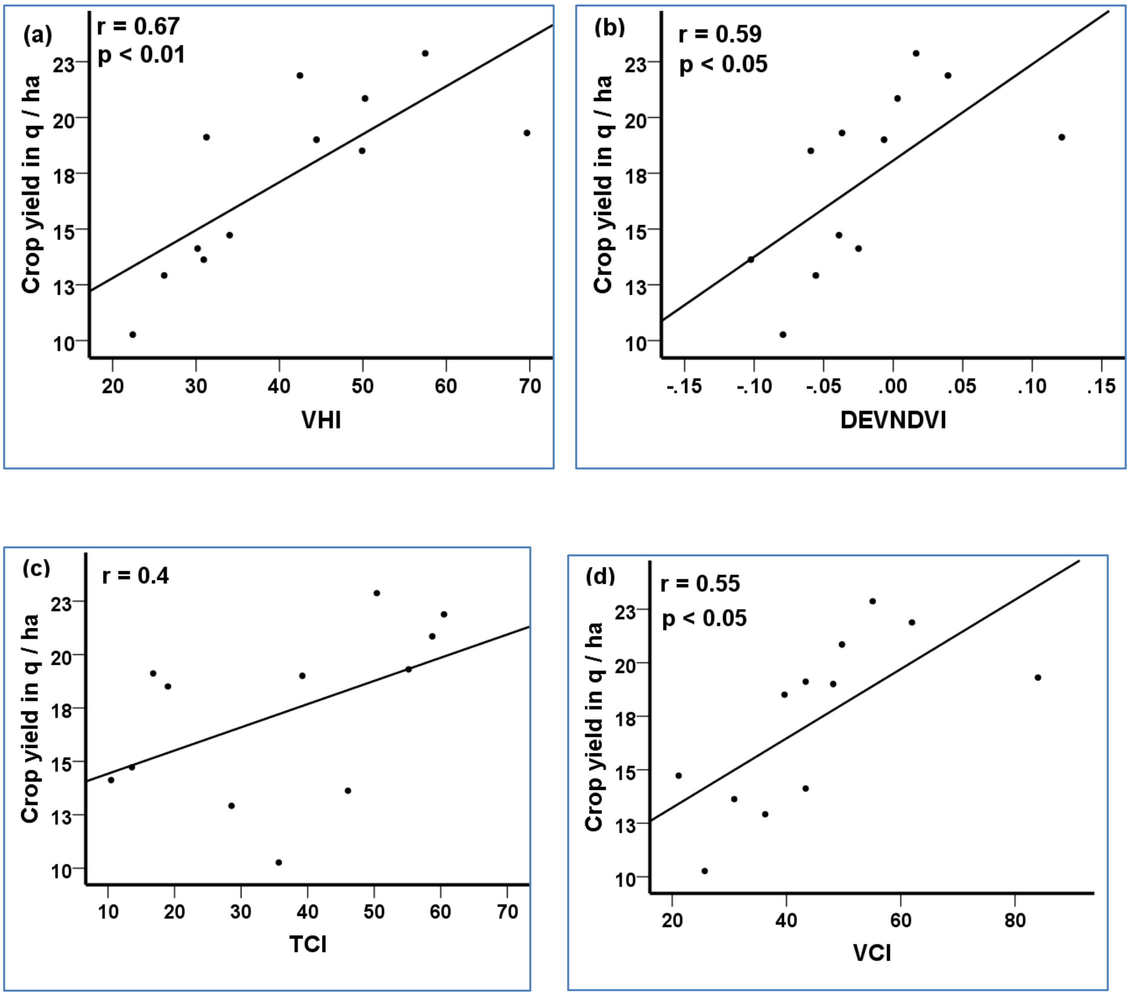

Figure 4.4: Scatter plots showing the relationship between crop yield and Landsat-based agricultural drought indices.

4.6 Identification of Suitable Remote sensing-based drought index from Landsat image

The performance comparison among Landsat-based agricultural drought indices obtained in Sections 4.1.1.4 and 4.1.1.5 is summarized in Table 4.2. When compared to other drought indices, the VHI has the best agreement with both SPEI and crop yield (r=0.63 and r=0.67, p<0.01), followed by DevNDVI (r=0.55 and r=0.59, p<0.05) and then VCI (r=0.48 and r=0.55, p<0.05), while the TCI has the worst agreement (r=0.44, p<0.05 and r=0.4) with both SPEI and crop yield respectively, (Table 4.2). Overall, the findings demonstrated that VHI is the most appropriate remote sensing-based agricultural drought index derived from Landsat images for measuring agricultural dryness in the study region, followed by DevNDVI and then VCI, and TCI.

Table 4.2**:** Performance comparison among Landsat-based agricultural drought indices using Pearson's Correlation Coefficient (r).

Variables	Performance Evaluation using r			
	Dev_{NDVI}	TCI	VCI	VHI
SPEI	0.55*	0.44*	0.48*	**0.63****
Crop yield	0.59*	0.4	0.55*	**0.67****
	**. Correlation is significant at the 0.01 level			
	*. Correlation is significant at the 0.05 level			

The highest correlation coefficient values are shown in bold.

4.7 Performance Comparison of MODIS and Landsat based Indices for Agricultural Drought characterization

Because the efficacy of remote sensing-based agricultural drought indices varies depending on sensor properties, drought indices calculated from Landsat and MODIS images were compared based on their agreement with SPEI and crop production (Figure 4.5 and Figure 4.6). However, this study only looked at the difference in spatial resolution between the two satellite data sets. The results reveal that each index calculated from the Landsat image has a greater association (correlation coefficient value) with SPEI than the indices computed from the MODIS image (Figure 4.5). Furthermore, based on their link with crop yield, the performance of drought indicators generated from both satellite images was compared (Figure 4.6). The findings demonstrated that drought indices computed from Landsat images had a greater relationship with crop production than the drought indices computed using the MODIS sensor (Figure 4.6).

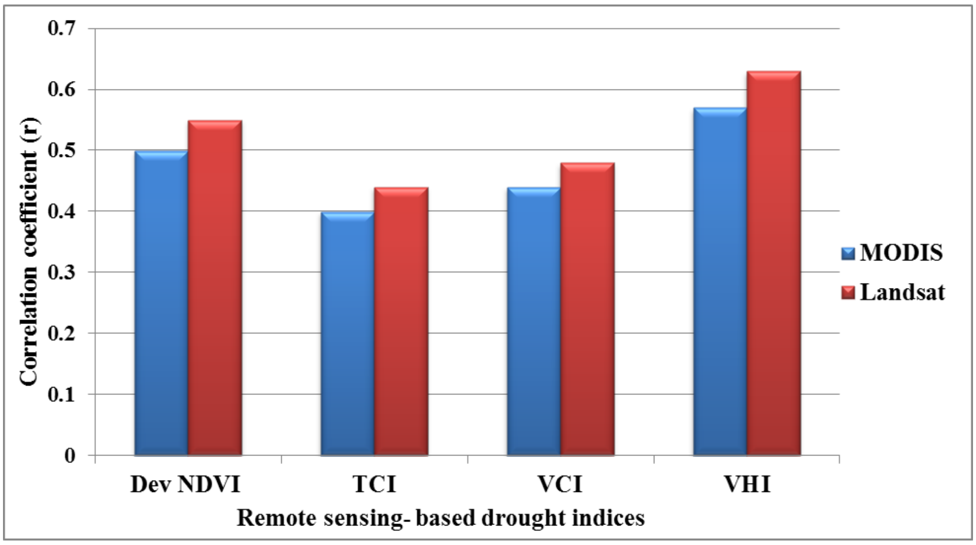

Figure 4.5: Performance comparison of MODIS and Landsat-based indices based on their agreement with SPEI using Pearson's Correlation Coefficient (r).

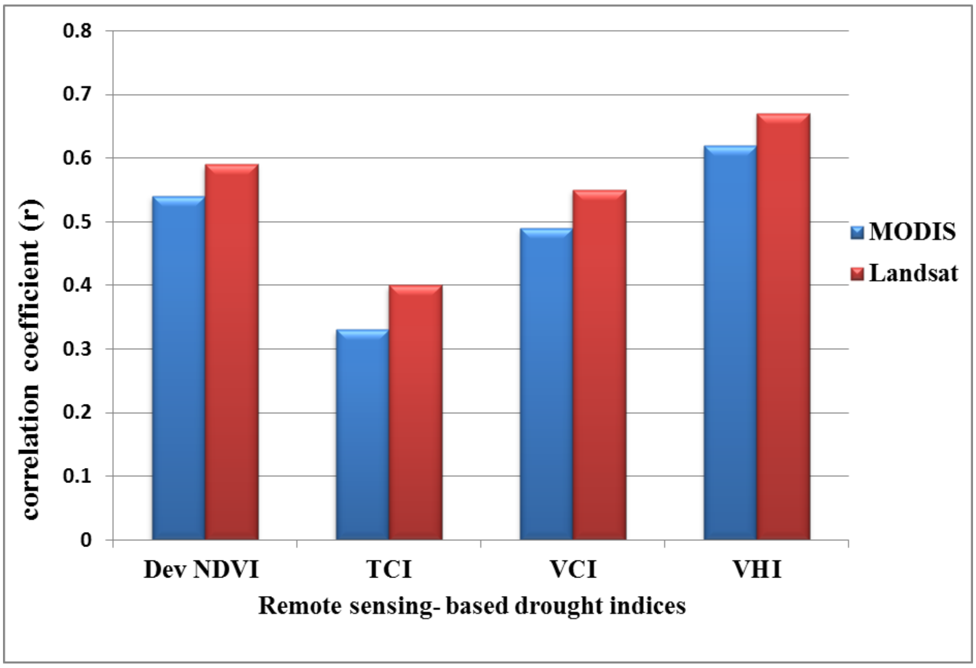

Figure 4.6: Performance comparison of MODIS and Landsat-based indices based on their agreement with crop yield using Pearson's Correlation Coefficient (r).

Overall, the comparison of MODIS and Landsat-based agricultural drought indices (Figure 4.5 and Figure 4.6) reveals that drought indices generated from Landsat data have a superior agreement with both SPEI and crop production.

Landsat images performed better for agricultural drought characterization, according to the findings. Furthermore, the agreement of VHI from the Landsat satellite image with SPEI and crop output was greater (r=0.63 and r=0.67, p<0.01) than other drought indicators (Table 4.2, Figure 4.5 and Figure 4.6). As a result, Landsat data may be used as a good satellite image for agricultural drought characterization, and VHI can be used as a suitable remote sensing-based drought index.

4.8 Drought Assessment using the Vegetation health index (VHI)

As shown in Section 4.1.2, VHI derived from Landsat images has a stronger relationship with SPEI and agricultural yield in the research region. Throughout the study period, the agricultural drought condition in the research region was examined using VHI from Landsat images as the best performing remote sensing-based agricultural drought indicator from the suitable sensor. Based on the VHI criterion, the drought severity level has been characterized as extreme, severe, moderate, mild, and no drought. The geographical pattern of agricultural drought for the years 2000 and 2005 was plotted using this measure (Figure 4.7 and Table 4.3).

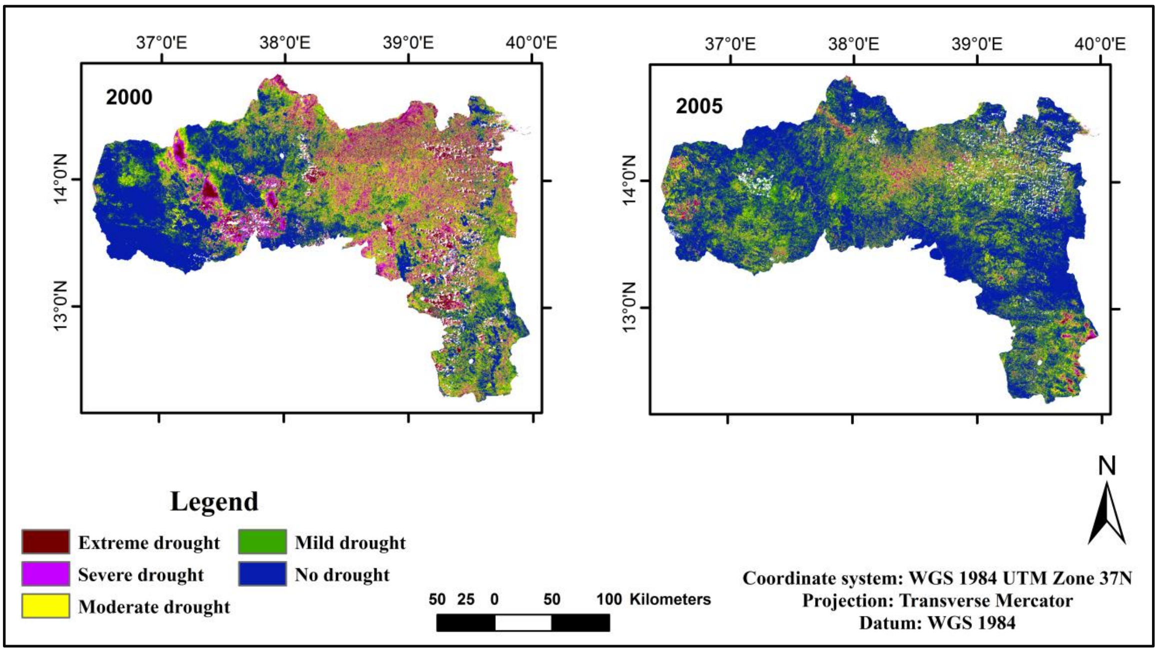

Figure 4.7: The spatial pattern of agricultural drought severity for the year 2000 and 2005.

In the year 2000, 52 percent of the study area in the western and southeastern regions of the research area had near-normal and normal vegetation conditions (Figure 4.7 and Table 4.3). Drought affected the central and northeastern halves of the study area, with moderate, severe, and extreme drought affecting 22, 15, and 6 percent of the study area, respectively (Table 4.3).

Table 4.3 Agricultural drought severity and areal coverage based on VHI for the years 2000 and 2005.

Drought severity level	Years			
	2000		2005	
	Area(ha)	Area (%)	Area (ha)	Area (%)
Extreme	316419	6	39793.68	1
Severe	786779.8	15	193261.3	4
Moderate	1145591	22	667140	13
Mild	1067978	20	1390080	26
No Drought	1708576	32	2825538	54
Non vegetated area	235,256	4	144,788	3
Total	5,260,600	100	5,260,600	100

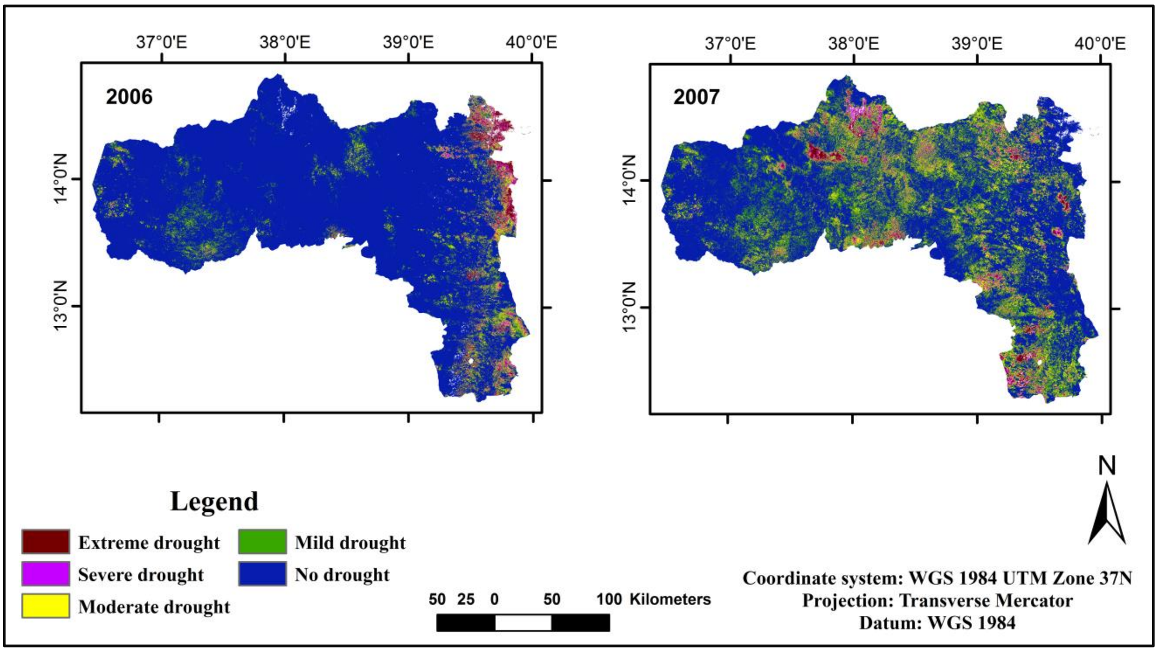

Figure 4.8: The spatial pattern of agricultural drought severity for the year 2006 and 2007.

Table 4.4: Agricultural drought severity and areal coverage based on VHI for the years 2006 and 2007.

Drought severity Level	Years 2006		2007	
	Area(ha)	Area (%)	Area (ha)	Area (%)
Extreme	75760.1	1	76515.8	1
Severe	122486.9	2	216224.9	4
Moderate	190502.5	4	551169.4	10
Mild	296243.1	6	1086881	21
No Drought	4526137	86	3277047	62
Non vegetated area	49,470	1	52,762	1
Total	5,260,600	100	5,260,600	100

In 2005, 2006, and 2007, the area impacted by severe and extreme agricultural drought decreased as compared to 2000 (Figure 4.7, Figure 4.8, Table 4.3, and Table 4.4). In the year 2005, around 54 and 26 percent of the research area showed normal and near-normal vegetation conditions while moderate, severe, and extreme degrees of agricultural drought afflicted 13, 4, and 1 percent of the study area, respectively (Figure 4.7 and Table 4.3). Contrary to this, very small portions of the research area (less than 8% of total areas) were affected by agricultural drought in the year 2006 (Figure 4.8 and Table 4.4). This year, 86 and 6 percent of the area has normal and near-normal vegetation conditions, respectively. This normal vegetation condition was decreased during 2007 and normal and near-normal condition was observed in 62 and 21 percent of the total area, respectively (Figure 4.8 and Table 4.4). In 2008 (Figure 4.9 and Table 4.5), 17 and 55 percent of the study area had near-normal and normal vegetation conditions, respectively. Drought affected the central and eastern halves of the research area, with moderate, severe, and extreme drought affecting 14, 9, and 4 percent of the study area, respectively (Figure 4.9 and Table 4.5).

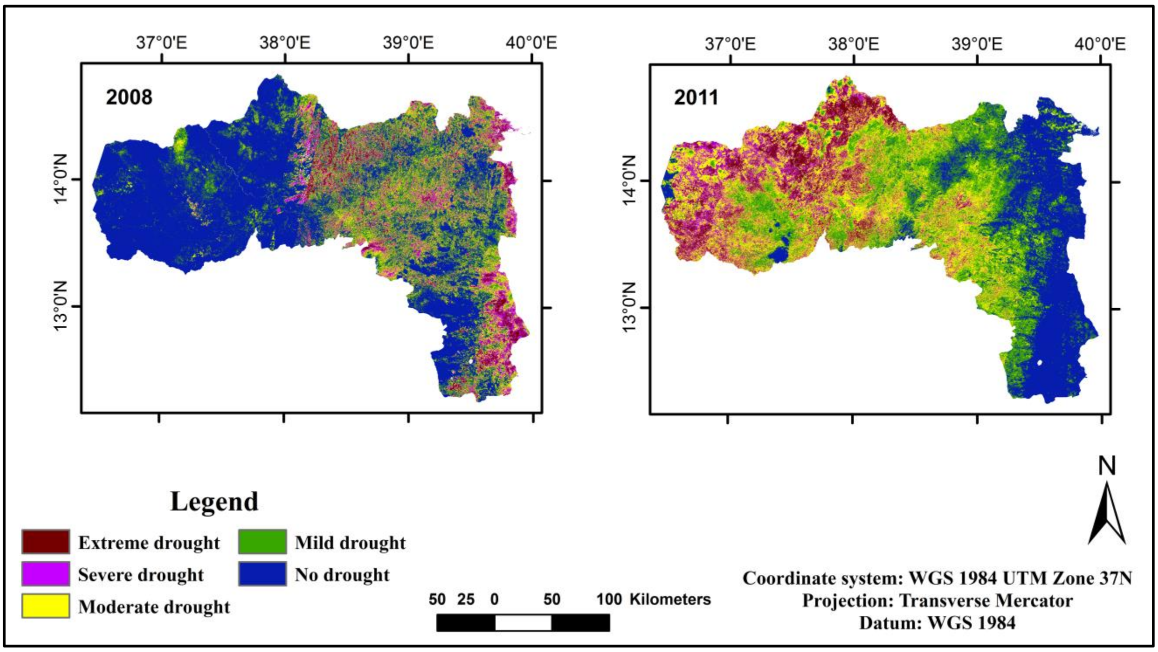

Figure 4.9: The spatial pattern of agricultural drought severity for the years 2008 and 2011.

Table 4.5: Agricultural drought severity and areal coverage based on VHI for the years 2008 and 2011.

Drought severity level	Years			
	2008		2011	
	Area (ha)	Area (%)	Area (ha)	Area (%)
Extreme	187806.5	4	462540.3	9
Severe	465859.3	9	595317.4	11
Moderate	742897.1	14	1434709	27
Mild	916249.8	17	1355658	26
No Drought	2902621	55	1399581	27
Non vegetated area	45,167	1	12,794	0
Total	5,260,600	100	5,260,600	100

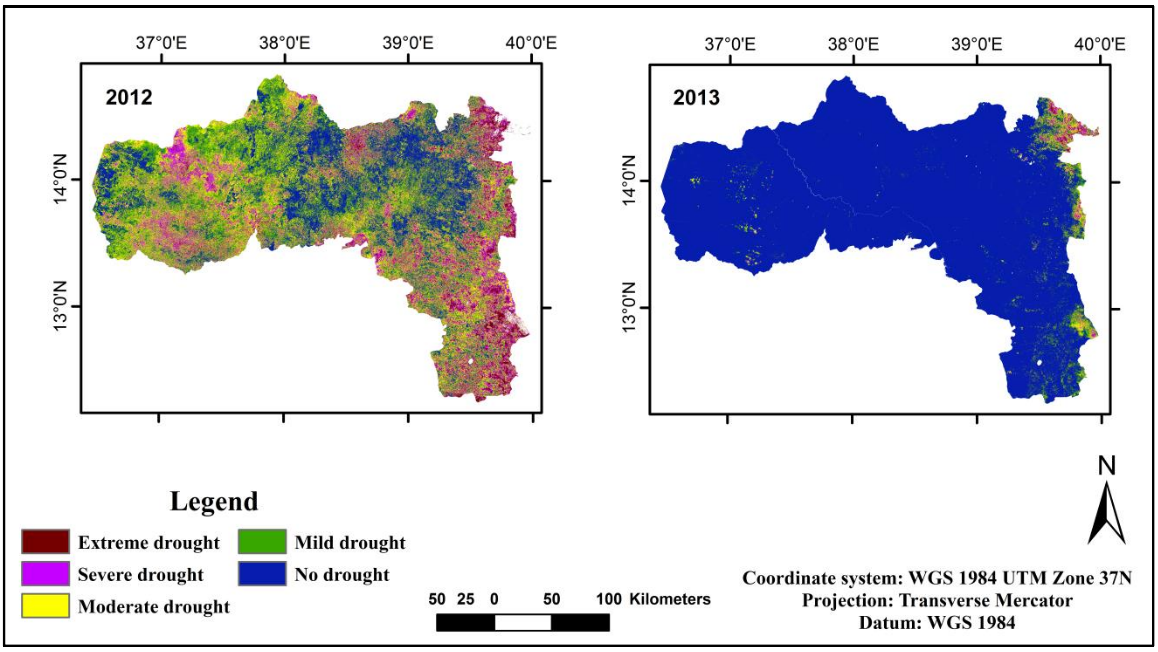

Figure 4.10: The spatial pattern of agricultural drought severity for the years 2012 and 2013.

Drought conditions were severe in the study region's western portion in 2011 (Figure 4.9 and Table 4.5). This year, agricultural droughts of moderate, severe, and extreme severity affected 27, 11, and 9 percent of the study area, respectively 2011 (Figure 4.9 and Table 4.5). However, in the research area's eastern regions, 26 percent and 27 percent of the total area, respectively, have near-normal and normal vegetation conditions 2011 (Figure 4.9 and Table 4.5).

Table 4.6Agricultural drought severity and areal coverage based on VHI for the years 2012 and 2013.

Drought severity level	Years			
	2012		2013	
	Area(ha)	Area (%)	Area (ha)	Area (%)
Extreme	317402	6	16756.5	0
Severe	814095.4	15	41535.3	1
Moderate	1377017	26	88630.4	2
Mild	1403992	27	149581.1	3
No Drought	1277952	24	4944019	94
Non vegetated area	70142	1	20,078	0
Total	5,260,600	100	5,260,600	100

Agricultural drought struck several eastern and western portions of the study area in 2012, as seen in Figure 4.10. During the year 2012, 53% of the research region displayed normal vegetation conditions while 26, 15%, 6% of the areas in the eastern and western portions of the region were afflicted by moderate, severe, and extreme drought, respectively (Figure 4.10 and Table 4.6). Contrary to this, a very little portion of the area (less than 4% of the total area) was affected by agricultural drought during 2013, whereas normal and near-normal condition was observed in 94 and 3 percent of the total area, respectively (Figure 4.10 and Table 4.6). However, the percentage of normal vegetation conditions was decreased in the year 2014 (Figure 4.11 and Table 4.7). In 2014, 63 and 13 percent of the total area reflects normal and near-normal vegetation conditions while moderate drought hit 9, 7, and 5 percent of the total study area, severe and extreme levels of agricultural drought, respectively (Figure 4.11 and Table 4.7).

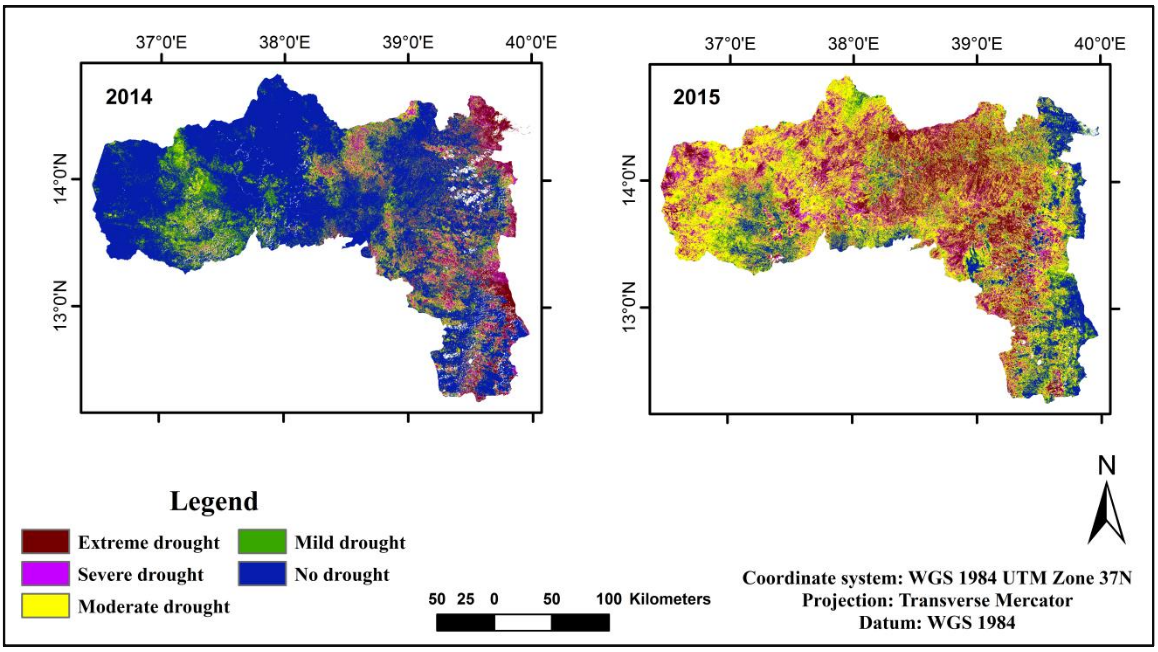

Figure 4.11: The spatial pattern of agricultural drought severity for the years 2014 and 2015.

In the year 2015, the bulk of the research region was struck by agricultural droughts ranging from moderate to high intensity, as shown in Figure 4.11and Table 4.7. During the research period, the proportion of land impacted by drought was greatest in 2015. This year, extreme, severe, and moderate drought affected 16, 17, and 43 percent of the region's northwestern, central, and northeastern regions, respectively (Figure 4.11and Table 4.7).

Besides, only a small portion (24%) of the area in the southwestern and southeastern parts shows near-normal vegetation conditions (Figure 4.11and Table 4.7).

Table 4.7 Agricultural drought severity and areal coverage based on VHI for the years 2014 and 2015.

Drought severity level	Years			
	2014		2015	
	Area(ha)	Area (%)	Area (ha)	Area (%)
Extreme	263753.2	5	830794.2	16
Severe	358540.6	7	880965.5	17
Moderate	489752.4	9	2263867	43
Mild	704938.1	13	562652.2	11
No Drought	3291747	63	678888.9	13
Non vegetated area	151,868	3	43,432	1
Total	5,260,600	100	5,260,600	100

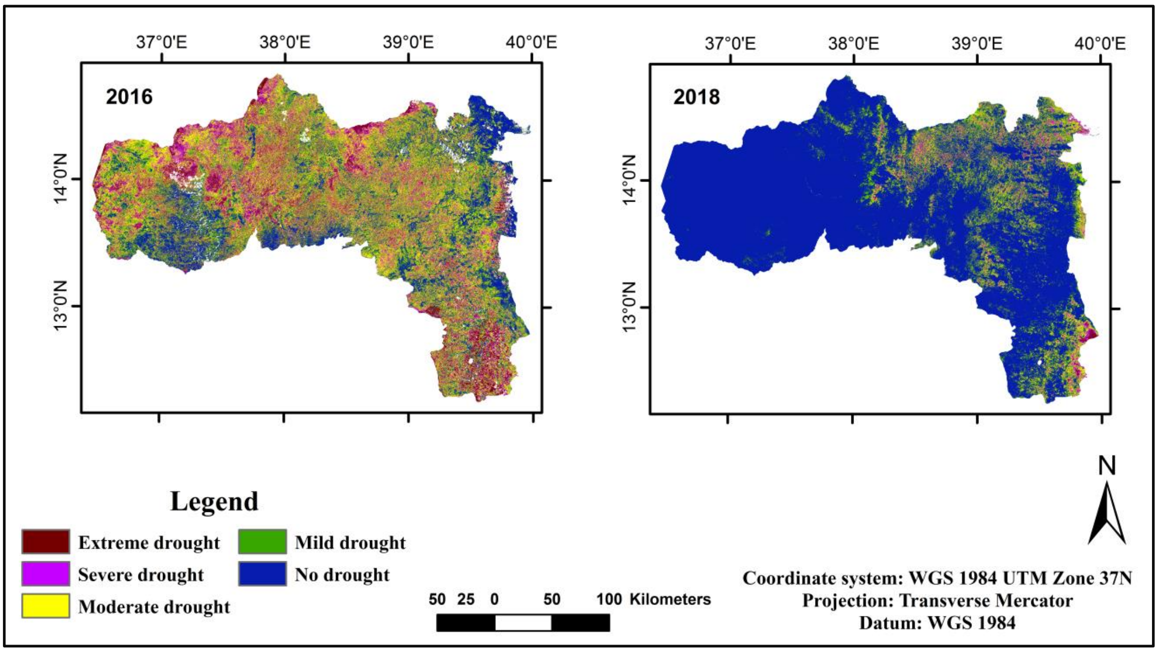

Figure 4.12: The spatial pattern of agricultural drought severity for the years 2016 and 2018.

Figure 4.12 and Table 4.8 show that in the year 2016, 19 and 17 percent of the research area had near-normal and normal vegetation conditions, respectively. Drought afflicted the majority of the study area, with moderate, severe, and extreme drought impacting 29, 18, and 12% of the study area, respectively (Table 4.8). On the contrary, during the year 2018, the majority of the research area is around 79 and 10% of the total area reflects normal and near-normal vegetation conditions (Figure 4.12 and Table 4.8). Drought hit 7 and 3% of the study region, respectively, with moderate and severe levels of drought (Figure 4.12 and Table 4.8).

Table 4.8: Agricultural drought severity and areal coverage based on VHI for the years 2016 and 2018.

Drought severity level	Years			
	2016		2018	
	Area(ha)	Area (%)	Area (ha)	Area (%)
Extreme	643595.8	12	25783.9	0
Severe	954071.5	18	149292.5	3
Moderate	1517145	29	359926.6	7
Mild	1013152	19	541225.6	10
No Drought	892635.2	17	4170275	79
Non vegetated area	240000	5	14,097	0
Total	5,260,600	100	5,260,600	100

CHAPTER FIVE

5. DISCUSSION

Because the efficacy of remote sensing-based agricultural drought indices varies among regions and sensor parameters, evaluating the usefulness of a given drought index for a specific location to help in agricultural drought monitoring is crucial. This study used MODIS and Landsat satellite images to compare and assess the usefulness of four remote sensing-based agricultural drought indicators for describing agricultural drought. The agreement of remote sensing-based agricultural indices derived from both satellite images and the in-situ-based drought index (SPEI) and crop output was investigated and compared. To evaluate the correlation between remote sensing-based indices and SPEI, as well as between remote sensing-based indices and crop yield, Pearson's Correlation Coefficient (r) was calculated. Each indicator acquired from both satellite photographs was found to be an effective, quick, and low-cost method for assessing agricultural dryness in the area. However, when it comes to analyzing agricultural dryness in the region, each indicator performs differently.

In the examination of drought indices using MODIS and Landsat images, the VHI, which is based on the additive combination of VCI and TCI, was shown to be superior to other drought indices (VCI, DevNDVI, and TCI), and was judged to be the best drought index for agricultural drought characterization. Because agricultural drought is caused by a wide range of causes, no one indicator can effectively reflect the intricacies and variety of drought conditions (Huang et al., 2018; Sun et al., 2020). As a result, various studies have shown that combining data from several indices might potentially improve drought monitoring (Amalo et al., 2017; Huang et al., 2018; Sun et al., 2020; Zhuo et al., 2016; Zhang et al., 2017). As a result, the VHI performed better than individual remote sensing-based drought indices thanks to the use of VCI, which measures the influence of moisture on vegetation, and TCI, which measures the effect of temperature on vegetation. This conclusion was consistent with prior research that found the VHI to be more capable of agricultural drought monitoring than the VCI and TCI (Amalo et al., 2017; Gidey et al., 2018b; Siburian, 2018; Zhuo et al., 2016).

Also, research has shown that combining numerous single remote sensing-based drought indices produce better results than using a single remote sensing-based drought index (Zhuo et al., 2016; Amalo et al., 2017; Zhang et al., 2017; Huang et al., 2018; Sun et al., 2020).

Furthermore, an examination of drought indices generated from both satellite images demonstrates that TCI is the least effective of the four drought indices in detecting agricultural drought. The explanation for this might be that remotely sensed drought indicators based on vegetative indices like NDVI are more sensitive to detecting drought in vegetation during the wet season than thermal indices like TCI, which are more sensitive to detecting drought in vegetation during the dry season (Kogan, 1995; Amalo et al., 2017; Nugraha et al., 2019). Furthermore, TCI's poor performance in identifying agricultural droughts may be due to the fact that it is calculated from land surface temperature, which is more effective in describing moisture and evaporative stresses in vegetation when combined with other vegetation indices such as NDVI than when used alone (Vyas et al., 2015). This conclusion was consistent with the findings of Thenkabail et al. (2004), who found Dev_{NDVI} and VCI to be more sensitive indicators for agricultural drought evaluation than TCI. Some research concluded that the VCI performed better than the TCI for drought monitoring in semi-arid areas, which backed up this assertion (Zhang and Jia, 2013; Siburian, 2018).

According to the study's findings, TCI had the lowest association with SPEI and agricultural output in both images. However, TCI from both images shows a positive link with SPEI and crop production. As a result, this discovery demonstrates that TCI can provide relevant data for characterizing agricultural drought. This corresponded to research that indicated the TCI can successfully monitor agricultural drought conditions (Kogan, 1995; Amalo et al., 2017; Nugraha et al., 2019). However, the findings of this study contradicted previous research conducted in humid and irrigated regions by Zhang et al.(2017) and Shad et al.(2017) respectively, that found the TCI and VCI to be unreliable drought indicators for agricultural drought monitoring. This might be owing to the belief that the performance of remote sensing-based drought indicators varies among regions.

Due to differences in sensor characteristics such as spatial resolution, the performance of remote sensing-based drought indices derived from MODIS images at 250 m spatial resolution and Landsat images at 30 m spatial resolution varies, the performance of drought indices computed from Landsat and MODIS images were compared in this study based on their agreement with SPEI and crop yield. All drought indices obtained from Landsat photos with a finer spatial resolution agree better with crop yield and SPEI than drought indices derived from MODIS images with a coarser spatial resolution, according to the findings. This suggests that Landsat images with a finer geographical resolution perform better for agricultural drought characterization than MODIS images with a coarser spatial resolution. Furthermore, this research showed that higher spatial resolution satellite images performed better for assessing agricultural droughts. When used to analyze agricultural dryness, remote sensing-based drought indices produced from finer spatial resolution images perform better and are more sensitive, according to prior studies (Hazaymeh and Hassan, 2016; Al-Bakri et al., 2018; Brema et al., 2019; Arekhi et al., 2020).

The findings of this study demonstrate that the maximum agreement (highest correlation coefficient values) was achieved when VHI from Landsat data was related to SPEI and crop production. As a consequence, this finding shows that Landsat data is a useful satellite image for assessing agricultural dryness in the research region and that VHI is the appropriate remote sensing-based agricultural drought index. The findings are in line with previous research that has shown that the VHI from a Landsat sensor may give accurate and trustworthy data for agricultural drought monitoring (Ghaleb et al., 2015; Brema et al., 2019; Siburian, 2018; Arekhi et al., 2020).

All remote sensing-based drought indices and the in-situ-based drought index (SPEI), as well as remote sensing-based drought indices and crop output, showed moderate to strong associations. Previous studies in the research area demonstrated a high level of concordance between remote sensing-based drought indices and crop yield, as well as in-situ-based drought indices (Gebrehiwot et al., 2011; Gidey et al., 2018b; Chere, 2019).

Throughout the study period, the VHI from the Landsat image was used to examine agricultural drought conditions in the research region. A wide variety of moderate to extreme agricultural drought conditions hit the area in the years 2000, 2011, 2012, 2015, and 2016. This allegation was supported by the findings of Gebrehiwot et al. (2011)'s study in the Tigray Region, which demonstrated that the region had experienced agricultural drought. The findings are also consistent with those of Eze et al. (2020), who discovered that droughts in 2015 and 2016 led to significant yield reductions in the region. During the years 2006, 2013, and 2018, only a small portion of the research region was hit by severe agricultural drought, while the bulk of the study area had near-normal or normal vegetation conditions. These findings are consistent with prior research, which found typical vegetation conditions in the study area in 2006, 2013, and 2018 (Liou and Mulualem, 2019; Chere, 2019).

CHAPTER SIX

6. CONCLUSION AND RECOMMENDATIONS

6.1 Conclusion

The goal of this study was to compare the performance of four remote sensing-based agricultural drought indices for agricultural drought characterization using MODIS and Landsat images in the Tigray Region. The drought indices compared in this study include NDVI deviation (DEVNDVI), Temperature Condition Index (TCI), Vegetation Condition Index (VCI), and vegetation health index (VHI). The concordance between remote sensing-based drought indices and in-situ-based drought indicators (SPEI) and agricultural output was studied.

When comparing the performance of MODIS-based drought indicators, the VHI beat the others, having the strongest correlation with SPEI and crop output, followed by DevNDVI, VCI, and TCI. VHI, followed by DevNDVI, VCI, and TCI, is the most suitable remote sensing-based agricultural drought indicator from the MODIS sensor for agricultural drought assessment. When Landsat-based drought indicators were compared, the VHI beat the others, with the greatest connection with SPEI and agricultural yield, followed by DevNDVI, VCI, and TCI. The most acceptable remote sensing-based drought indices from Landsat images for agricultural drought evaluation are VHI, followed by DevNDVI, VCI, and TCI, according to this study.

The performance of drought indices derived from MODIS images at 250 m spatial resolution and Landsat images at 30 m spatial resolution varies due to differences in sensor characteristics such as spatial resolution. This study compared the performance of MODIS and Landsat-based indices based on their agreement with SPEI and crop yield. All indices obtained from Landsat images with a finer geographic resolution agree better with crop yield and SPEI than indices derived from MODIS images with a coarser spatial resolution, according to the findings. As a result of this finding, it was discovered that remote sensing-based drought indices produced from Landsat images with a greater spatial resolution worked better for assessing agricultural drought in the region.

Furthermore, the findings of this study demonstrate that the highest agreement was obtained when VHI from Landsat satellite images was connected with SPEI and crop output. As a consequence, the Landsat satellite image has been judged to be the best satellite image for agricultural drought evaluation, and the VHI is the best remote sensing-based agricultural drought indicator.

During the study period, the research region's agricultural drought situation was assessed using VHI from a Landsat sensor as the best remote sensing-based drought indicator from an applicable sensor. The area was subjected to a wide range of moderate to serious agricultural drought conditions in the years 2000, 2011, 2012, 2015, and 2016, according to the findings. However, only a tiny fraction of the research region was affected by extreme and severe agricultural drought in the years 2006, 2013, and 2018, while the rest of the study area had near-normal and normal vegetation conditions.

6.2 Recommendations

The following recommendations for further research are made based on the findings of this study:

- Future studies should look at the possibilities of quantifying agricultural dryness using other remote sensing-based drought indices derived from additional reflectance bands.
- In future studies for agricultural drought evaluation, other high spatial resolution images, such as sentinel, should be examined.
- VHI has higher performance for agricultural drought characterization, according to the conclusions of this study. Therefore, stakeholders working on drought might use VHI as a drought early warning system to increase farmers' access to drought predictions, allowing them to implement effective drought coping methods on time.
- Improved agricultural technologies and information such as irrigation, drought-tolerant crops, conservation crop rotations, and water and soil moisture conservation practices should be made to mitigate the adverse effects of the drought on agriculture and the economy.

References

Al-Bakri, J. T., Al-Khreisat, A., Shawash, S., Qaryouti, E., and Saba, M. (2018). Assessment of remote sensing indices for drought monitoring in Jordan. *Asian Journal of Geoinformatics, 17*(3).

Alemu, T., and Yoseph, G. (2004). Provision of seeds to drought affected people in eastern and central Tigray: an evaluation. Report for Project Implemented by CISP/REST, Funded by USAID-ODFA, Makelle, Ethiopia.

Alexandrov, V. A., and Hoogenboom, G. (2000). The impact of climate variability and change on crop yield in Bulgaria. *Agricultural and Forest Meteorology, 104*, 315-327.

Amalo, L. F., Hidayat, R., and Haris. (2017). Comparison between remote-sensing-based drought indices in East Java. IOP Conference Series: Earth and Environmental Science, 54, 012009.

Arekhi, M., Saglam, S., and Ozkan, U. Y. (2020). Drought monitoring and assessment using Landsat TM/OLI data in the agricultural lands of Bandar-e-Turkmen and Gomishan cities, Iran. *Journal of Environment, Development and Sustainability, 22*(7), 6691-6708.

Armanuos, A. M., Al-Ansari, N., and Yaseen, Z. M. (2020). Cross Assessment of Twenty-One Different Methods for Missing Precipitation Data Estimation. *Atmosphere, 11*(4), 389.

Artis, D. A., and Carnahan, W. H. (1982). Survey of emissivity variability in thermography of urban areas. *Remote Sensing of Environment, 12*(4), 313-329.

Asheber, S., A. (2010). Mitigating Drought: Policy Impact Evaluation, A Case of Tigray Region, Ethiopia. *Unpublished MSc Thesis, International institute for geo-information science and earth observation Enschede, the Netherlands*.

Awojobi, O. N., and Tetteh, J. (2.017). The Impacts of Climate change in Africa: A Review of the scientific literature. International academic research for multidisciplinary, 5(11), 2320-5083.

Bannari, A., Morin, D., Bonn, F., and Huete, A. (1995). A review of vegetation indices. *Remote sensing reviews, 13*(1-2), 95-120.

Bandyopadhyay, N., and Saha, A. K. (2016). A comparative analysis of four drought indices using geospatial data in Gujarat, India. *Arabian Journal of Geosciences, 9*(5), 341.

Beguería, S., Vicente-Serrano, S. M., Reig, F., and Latorre, B. (2014). Standardized precipitation evapotranspiration index (SPEI) revisited: parameter fitting, evapotranspiration models, tools, datasets and drought monitoring. *International Journal of Climatology, 34*(10), 3001-3023.

Berhan, G., Tadesse, T., Atnafu, S., and Hill, S. (2011). Drought Monitoring in Food-Insecure Areas of Ethiopia by Using Satellite Technologies. *In Experiences of Climate Change Adaptation in Africa*, 183-200.

Bhuiyan, C., Saha, A., Bandyopadhyay, N., and Kogan, F. (2017). Analyzing the impact of thermal stress on vegetation health and agricultural drought–a case study from Gujarat, India. *GIScience and Remote Sensing, 54*(5), 678-699.

Brema, J., Rahul, T., and Julius, J. J. (2019). Study on Drought Monitoring Based on Spectral Indices in Noyyal River Sub-watershed Using Landsat-8 Imageries. *Paper presented at the Proceedings of International Conference on Remote Sensing for Disaster Management.*

Chander, G., Markham, B. L., and Helder, D. L. (2009). Summary of current radiometric calibration coefficients for Landsat MSS, TM, ETM+, and EO-1 ALI sensors. *Remote Sensing of Environment, 113*(5), 893-903.

Chavez, P. S. (1996). Image-based atmospheric corrections-revisited and improved. *Photogrammetric engineering and remote sensing, 62*(9), 1025-1035.

Chere, Z. (2019). Spatio-temporal dynamics of agricultural drought and soil organic carbon in the highlands of Ethiopia. *Msc thesis submitted to the department of geography and environmental studies of addis ababa university*.

Coll, C., Galve, J. M., Sanchez, J. M., and Caselles, V. (2010). Validation of Landsat-7/ETM+ Thermal-Band Calibration and Atmospheric Correction With Ground-Based Measurements. *IEEE Transactions on Geoscience and Remote Sensing, 48*(1), 547-555.

CSA. (2008). Summary and Statistical Report of the 2007 Population and Housing Census, Federal Democratic Republic of Ethiopia Population Census Commission.

CSA. (2018). Area and production of major crops. 1-140.

Dai, A. (2011). Drought under global warming: a review. *Wiley Interdisciplinary Reviews: Climate Change, 2*(1), 45-65.

Dalezios, N. R., Gobin, A., Alfonso, A. M. T., and Eslamian, S. (2017). Agricultural drought indices: combining crop, climate, and soil factors. In *Handbook of Drought and Water Scarcity* (pp. 73-89): CRC Press.

Delbiso, T. D., Rodriguez-Llanes, J. M., Donneau, A. F., Speybroeck, N., and Guha-Sapir, D. (2017). Drought, conflict and children's undernutrition in Ethiopia 2000-2013: a meta-analysis. *Bull World Health Organ, 95*(2), 94-102. doi:10.2471/BLT.16.172700

Dewi, E. K., and Trisakti, B. (2017). Comparing atmospheric correction methods for Landsat OLI data. *International Journal of Remote Sensing and Earth Sciences (IJReSES), 13*(2), 105-120.

Didan, K., Munoz, A. B., Solano, R., and Huete, A. (2015). MODIS vegetation index user's guide (MOD13 series).

Eshetie, S. M., Demisse, G., and Suryabhagavan, K. V. (2016). Evaluation of vegetation indices for agricultural drought monitoring in East Amhara, Ethiopia. *International Journal of Scientific Research, 5*(10), 535 - 540.

Evans, J. D. (1996). *Straightforward statistics for the behavioral sciences*: Thomson Brooks/Cole Publishing Co.

Eze, E., Okolo, C. C., and Negash, E. (2020). Yield and yield-reduction in recent drought years in southern Tigray, northern Ethiopia: Implications on food security.

Gao, B. C. (1996). NDWI—A normalized difference water index for remote sensing of vegetation liquid water from space. Remote sensing of environment, 58(3), 257-266.

Ganie, M., and Nusrath, D. A. (2016). Determining the Vegetation Indices (NDVI) from Landsat 8 Satellite Data. *International Journal of Advanced Research, 4*(8), 1459-1463.

Gebrehiwot,T., and van der Veena, A.(2013). Assessing the evidence of climate variability in the northern part of Ethiopia. *Journal of Development and Agricultural Economics, 5*(3), 104-119.

Gebrehiwot,T.,van der Veena, A., and Maathuisb, B. (2011). Spatial and temporal assessment of drought in the Northern highlands of Ethiopia. *International Journal of Applied Earth Observation and Geoinformation, 13*, 309-321.

Gidey, E., Dikinya, O., Sebego, R., Segosebe, E., and Zenebe, A. (2018a). Analysis of the long-term agricultural drought onset, cessation, duration, frequency, severity and spatial extent using Vegetation Health Index (VHI) in Raya and its environs, Northern Ethiopia. *Environmental Systems Research, 7*(13), 1-18.

Gidey, E., Dikinya, O., Sebego, R., Segosebe, E., and Zenebe, A. (2018b). Using Drought indices to model the statistical relationships between meteorological and agricultural drought in Raya and its environs, Northern Ethiopia. *Earth Systems and Environment, 2*(2), 265-279.

Gedif, B., Legesse, H., Solomon, A., and Suryabhagavan, K. V. (2014). Drought Risk Assessment using Remote Sensing and GIS: The Case of Southern Zone, Tigray Region, Ethiopia. *Journal of Natural Sciences Research*, 4(23), 87- 94.

GEOGLAM. (2019). The Group on Earth Observations Global Agricultural Monitoring Initiative, GEOGLAM Crop Monitor for Early Warning calendars.

Ghaleb, F., Mario, M., and Sandra, A. N. (2015). Regional landsat-based drought monitoring from 1982 to 2014. *Climate*, *3*(3), 563-577.

Haile, M. (2005). Weather patterns, food security and humanitarian response in sub-Saharan Africa. Philosophical Transactions of the Royal Society B: Biological Sciences, 360(1463), 2169-2182.

Heim, R. J. (2002). A review of twentieth-century drought indices used in the United States. *American Meteorological Society, 83*(8), 1149-1165.

Huang, J., Zhuo, W., Li, Y., Huang, R., Sedano, F., Su, W., Zhang, X. (2018). Comparison of three remotely sensed drought indices for assessing the impact of drought on winter wheat yield. *International Journal of Digital Earth*, *13*(4), 504-526.

Huang, S., Tang, L., Hupy, J. P., Wang, Y., and Shao, G. (2020). A commentary review on the use of normalized difference vegetation index (NDVI) in the era of popular remote sensing. *Journal of Forestry Research*, 1-6.

Hazaymeh, K., and Hassan, Q. K. (2016). Remote sensing of agricultural drought monitoring: A state of art review. AIMS Environ. Sci, 3, 604-630.

Horion, S., Carrão, H., Singleton, A., Barbosa, P., and Vogt. (2012). JRC experience on the development of Drought Information Systems. Europe, Africa and Latin America. EUR, 25235.

Hosking, J. R. M., and Wallis, J. R. (2005). *Regional frequency analysis: an approach based on L-moments*: Cambridge university press.

Hunt, E. R., and Rock, B. N. (1989). Detection of changes in leaf water content using near-and middle-infrared reflectance. Remote sensing of environment, 30(1), 43-54.

Jang, J. D., Viau, A. A., & Anctil, F. (2006). Thermal-water stress index from satellite images. International Journal of Remote Sensing, 27(8), 1619-1639.

Jeyaseelan, A. (2003). Droughts and floods assessment and monitoring using remote sensing and GIS. *Satellite remote sensing GIS applications in agricultural meteorology*, *291*.

Kogan, F. N. (1990). Remote sensing of weather impacts on vegetation in non-homogeneous areas. *International journal of remote sensing, 11*(8), 1405-1419.

Kogan, F. N. (1995). Application of vegetation index and brightness temperature for drought detection. *Adw. Space Res, 15,* 91- 100.

Kogan, F. N. (1997). Global Drought Watch from Space. *Bulletin of the American Meteorological Society, 78,* 621-636.

Kogan, F. N. (2001). Operational space technology for global vegetation assessment. *Bulletin of the American Meteorological Society, 82*(9), 1949-1964.

Kozanis, S., Christofides, A., Mamassis, N., Efstratiadis, A., and Koutsoyiannis, D. (2005). Hydrognomon: A hydrological data management and processing software tool. *Paper presented at the Geophysical Research Abstracts*.

Lambin, E. F., and Ehrlich, D. (1996). The surface temperature-vegetation index space for land cover and land-cover change analysis. International journal of remote sensing, 17(3), 463-487.

Legesse, G., and Suryabhagavan, K.V. (2014). Remote sensing and GIS based agricultural drought assessment in East Shewa Zone, Ethiopia, *Tropical ecology, 55(3)*, 349-363.

Leon, D. G., Contreras, S., and Hunink, J. (2019). Comparison of meteorological and satellite-based drought indices as yield predictors of Spanish cereals. *Agricultural Water Management, 213*, 388-396.

Liou, Y.A., and Mulualem, G. M. (2019). Spatio–temporal assessment of drought in Ethiopia and the impact of recent intense droughts. *Remote Sensing*, *11*(15), 1828.

Lyon, B. (2014). Seasonal drought in the Greater Horn of Africa and its recent increase during the March–May long rains. *Climate*, 27(21), 7953-7975.

Macarof, P., Groza, S., and Statescu, F. (2018). Investiganting Correlation LST and Vegetation Indices Using Landsat Images for the Warmest Month: A Case Study of Iasi County. *Annals of Valahia University of Targoviste, Geographical Series, 18*(1), 33-40.

Masih, I., Maskey, S., Mussá, F., and Trambauer, P. (2014). A review of droughts on the African continent: a geospatial and long-term perspective. *Journal of Hydrology Earth System Sciences*, *18*(9), 3635-3649.

Melese, A. (2016). Remote sensing and gis based drought vulnerability assessment: A case of Afar Regional State, Ethiopia. *Msc thesis submitted to the School of Graduate Studies of Addis Ababa University In partial Fulfillment of the requirements for the Degree of Masters of Science in Remote Sensing and Geoinformatics*.

Meyer, S. J., Hubbard, K. G., Wilhite, D. A., & Center, H. P. C. (1991). A crop-specific drought index for corn: I. Model development and validation. Climate Research at Regional Climate Centers in 1991, 55(2), 80.

Minamiguchi, N. (2005). The application of geospatial and disaster information for food insecurity, agricultural drought monitoring, and assessment by the FAO GIEWS and Asia FIVIMS. *Workshop on reducing food insecurity associated with natural Paper presented at the IOP Conference Series*: Earth and Environmental Science.*disasters in Asia and the Pacific*. Bangkok, Thailand.

Mishra, A. K., and Singh, V. P. (2010). A review of drought concepts. *Journal of Hydrology*, 391(1-2), 202-216.

Morid, S., Smakhtin, V., and Moghaddasi, M.(2006). Comparison of seven meteorological indices for drought monitoring in Iran. *International Journal of Climatology*, *26*(7), 971-985.

Narasimhan, B., & Srinivasan, R. (2005). Development and evaluation of Soil Moisture Deficit Index (SMDI) and Evapotranspiration Deficit Index (ETDI) for agricultural drought monitoring. Agricultural and forest meteorology, 133(1-4), 69-88.

Nugraha, A., Gunawan, T., and Kamal, M. (2019). *Comparison of Land Surface Temperature Derived from Landsat 7 ETM+ and Landsat 8 OLI/TIRS for Drought Monitoring.*

Nwilo, P., Umar, A., Adepoju, M., and Okolie, C. (2019). Spatio-Temporal Assessment of Changing Land Surface Temperature and Depleting Water in the Lake Chad Area. *South African Journal of Geomatics, 8*(2), 144-159.

Owrangi, M. A., Adamowski, J., Rahnemaei, M., Mohammadzadeh, A., & Sharifan, R. A. (2011). Drought monitoring methodology based on AVHRR images and SPOT vegetation maps. *Journal of water resource and protection*, *3*(05), 325-334.

Palmer, W. C. (1968). Keeping track of crop moisture conditions, nationwide: the new crop moisture index. *Weather wise* 21: 156-161.

Panu, U. S., and Sharma, T. C. (2002). Challenges in drought research: some perspectives and future directions. *Hydrological Sciences, 47*, 19-30.

Psomiadis, E., Dercas, N., Dalezios, N. R., and Spyropoulos, N. V. (2017). Evaluation and cross-comparison of vegetation indices for crop monitoring from sentinel-2 and worldview-2 images. *Paper presented at the Remote Sensing for Agriculture, Ecosystems, and Hydrology XIX.*

Qamer, F. M., Krupnik, T. J., Pandey, P. R., and Ahmad, B. (2019). Resource book: Earth observation and climate data analysis for agricultural drought monitoring in South Asia.

Rhee, J., Im, J., and Carbone, G. (2010). Monitoring agricultural drought for arid and humid regions using multi-sensor remote sensing data. *Remote Sensing of environment*, *114*(12), 2875-2887.

Shad, M. S., Ildoromi, A., and Akhzari, D. (2017). Drought Monitoring Using Vegetation Indices and MODIS Data (Case Study: Isfahan Province, Iran). *Journal of Rangeland Science, 7*(2), 148.

Siburian, I. M. (2018). Drought monitoring and assessment for agriculture area using remote sensing and hydrometeorological indices in WEST JAVA , INDONESIA. *Unpublished MSc Thesis,UNESCO-IHE Institute for Water Education, Delft, the Netherlands.*

Sobrino, J. A., Jiménez-Muñoz, J. C., and Paolini, L. (2004). Land surface temperature retrieval from LANDSAT TM 5. *Remote Sensing of Environment, 90*(4), 434-440.

Stagge, J. H., Tallaksen, L. M., Xu, C. Y., and Van Lanen, H. A. (2014). Standardized precipitation-evapotranspiration index (SPEI): Sensitivity to potential evapotranspiration model and parameters. *Paper presented at the Hydrology in a Changing World.*

Sun, X., Wang, M., Li, G., and Wang, Y. (2020). Regional-scale drought monitor using synthesized index based on remote sensing in northeast China. *Open Geosciences, 12*(1), 163-173.

Tefera, A., Ayoade, J., and Bello, N. (2019). Drought Occurrence Pattern in Tigray Region, Northern Ethiopia. *Journal of Applied Sciences and Environmental Management, 23*(7), 1341-1348.

Teillet, P., Staenz, K., and William, D. (1997). Effects of spectral, spatial, and radiometric characteristics on remote sensing vegetation indices of forested regions. *Remote Sensing of Environment, 61*(1), 139-149.

Temam, D., Uddameri, V., Mohammadi, G., Hernandez, E. A., and Ekwaro-Osire, S. (2019). Long-term drought trends in Ethiopia with implications for dryland agriculture. *J Water, 11*(12), 2571.

Teweldebirhan, T., Uddameri, V., Forghanparast, F., Hernandez, E. A., and Ekwaro-Osire, S. (2019). Comparison of meteorological-and agriculture-related drought indicators across ethiopia. *Water, 11*(11), 2218.

Thenkabail, P. S., Gamage, M., and Smakhtin, V. U. (2004). The use of remote sensing data for drought assessment and monitoring in Southwest Asia. (Vol. 85): Iwmi.

Thornthwaite, C. W. (1948). An approach toward a rational classification of climate. *Geographical review, 38*(1), 55-94.

Tian, L., Yuan, S., and Quiring, S. M. (2018). Evaluation of six indices for monitoring agricultural drought in the south-central United States. *Agricultural and Forest Meteorology, 249*, 107-119.

Tierney, J. E., Smerdon, J. E., Anchukaitis, K. J., and Seager, R. (2013). Multi-decadal variability in East African hydro-climate controlled by the Indian Ocean. *Nature*, 493(7432), 389.

Todisco, F., Vergni, L., and Mannocchi, F. (2008). An evaluation of some drought indices in the monitoring and prediction of agricultural drought impact in central Italy. *Irrigation in Mediterranean Agriculture: challenges and innovation for the next decades, 84*, 203-211.

Tucker, C. (1979). Red and photographic infrared linear combinations for monitoring vegetation. *Remote Sensing of Environment, 8*(2), 127-150.

USGS. (2015). Thematic Mapper Plus (ETM+) Level 1 (L1) Data Format Control Book (DFCB). 1-36.

USGS. (2016). Landsat 8 (L8) Data Users Handbook. 1-114.

USGS. (2019). Landsat 7 (L7) Data Users Handbook. 1-151.

Vicente-Serrano, S. M., Beguería, S., and López-Moreno, J. I. (2010). A Multiscalar Drought Index Sensitive to Global Warming: The Standardized Precipitation Evapotranspiration Index. *Journal of Climate*, *23*(7), 1696-1718.

Vicente-Serrano, S. M., Beguería, S., Lorenzo-Lacruz, J., Camarero, J.J., Lo´pez-Moreno, J., Azorin-Molina, C., Revuelto, J., Mora´n-Tejeda, E., and Sanchez-Lorenzo, A. (2012). Performance of Drought Indices for Ecological, Agricultural and Hydrological Applications. Earth Interactions, 16(10), 1-27.

Vyas, S., Bhattacharya, B. K., Nigam, R., Guhathakurta, P., Ghosh, K., Chattopadhyay, N., and Gairola, R. M. (2015). A combined deficit index for regional agricultural drought assessment over semi-arid tract of India using geostationary meteorological satellite data. *International Journal of Applied Earth Observation Geoinformation*, *39*, 28-39.

Wable, P. S., Jha, M. K., and Shekhar, A. (2018). Comparison of drought indices in a semi-arid river basin of India. *Water Resources Management*.

Wan, Z. (2006). MODIS land surface temperature products users' guide. *ICESS, University of California*.

Wang, Q., Wu, J., Lei, T., He, B., Wu, Z., Liu, M., and Zhou, H. (2014). Temporal-spatial characteristics of severe drought events and their impact on agriculture on a global scale. *Journal of Quaternary International*, *349*, 10-21.

Weldearegay, S. K., and Tedla, D. G. (2018). Impact of climate variability on household food availability in Tigray, Ethiopia. *Agriculture and Food Security*, *7*(1), 1-9.

Workie, T. G., and Debella, H. J. (2018). Climate change and its effects on vegetation phenology across ecoregions of Ethiopia. *Journal of Global Ecology Conservation*, *13*, 1-13.

Zargar, A., Sadiq, R., Naser, B. and Khan, F. I. (2011). A Review of Drought Indices. *Environmental Reviews*, *19*(1), 333-349.

Zeng, N. (2003). Drought in the Sahel. *Journal of Science*, *302*(5647), 999-1000.

Zhang, A., and Jia, G. (2013). Monitoring meteorological drought in semiarid regions using multi-sensor microwave remote sensing data. *Remote Sensing of Environment*, 134, 13-23.

Zhang, D., Wang, G. and Zhou, H. (2011a). Assessment on agricultural drought risk based on variable fuzzy sets model. *Chinese Geographical Science*, 21(2):167 175.

Zhang, Z., He, G., and Wang, X. (2010). A practical DOS model-based atmospheric correction algorithm. *International journal of remote sensing, 31*(11), 2837-2852.

Zhang, L., Jiao, W., Zhang, H., Huang, C., and Tong, Q. (2017).Studying drought phenomena in the Continental United States in 2011 and 2012 using various drought indices. *Remote Sensing of Environment*, 190, 96-106.

Zhang, X. P, Rong, F. L., Sheng, L., Quna, F. and Xiao, X. W. (2011b) The Study of Dynamic Monitor of Rice Drought in Jiang xi Province with Remote Sensing. *Procedia Environmental Science*, 10:1847–1853

Appendices

Appendix A: Cultivated area and total agricultural production of the major cereal crops in Tigray Region from 2000 to 2018.

Year	Area in hectare	Production in quintal
2000	535.2	5494.5
2005	585847.1	7568135.3
2006	705454.9	9612887.0
2007	709835.7	10026217.8
2008	707376.4	10415273.0
2011	716178.9	13254244.7
2012	730755.9	13887383.3
2013	758746.0	14649461.2
2014	765112.4	15954457.6
2015	752292.9	14380790.8
2016	778119.6	17025830.1
2018	785099.8	17957074.1

Source: Central Statistics Agency of Ethiopia

Appendix B: Name and location of weather stations in the study area

The selected stations for this study are highlighted in bold.

N.O	Station Name	Easting	Northing
1	**Abi Adi**	**13.6**	**39**
2	Adi-remeth	13.75	37.32
3	**Adigrat**	**14.28**	**39.45**
4	Adiwala	14.11	38.99
5	**Adwa**	**14.18**	**38.88**
6	**Alamata (Agr)**	**12.31**	**39.41**
7	Atsibe	13.88	39.74
8	**Axum**	**14.11**	**38.73**
9	Chercher	12.54	39.77
10	Dewehan	14.51	39.56
11	Dima	13.68	38.32
12	Edegaselus	14.09	39.69
13	**Endabaguna**	**13.94**	**38.18**
14	Feresmai	14.17	39.1
15	Finarwa	14.17	39.03
16	Fireweini	14.07	39.57
17	**Hagere Selam**	**13.65**	**39.17**
18	**Hawzen**	**13.97**	**39.43**
19	Hiwane	13.97	39.5
20	**Humera (Old)**	**14.10**	**36.52**
21	Ketemaneguse	14.12	37.41
22	**Korem**	**12.51**	**39.52**
23	Kunaba	13.97	39.87
24	**Maichew**	**12.79**	**39.55**
25	Maytsebry	13.56	38.14
26	**Mekele (AP)**	**13.47**	**39.53**
27	Mekele (obs)	13.52	39.47
28	Mugulat	14.11	39.35
29	**Seleklaka**	**14.11**	**38.48**
30	Semema	13.6	38.34
31	Sheket	13.35	39.75
32	Shiraro	14.4	37.76
33	**Shire Endasilasse**	**14.1**	**38.3**
34	Tekeze Hydro power	13.36	38.77
35	**Waja**	**12.28**	**39.6**
36	Wedisemro	12.76	39.34
37	**Wukro**	**13.83**	**39.6**
38	Yechila	13.28	38.99

(Source: National Meteorological Agency of Ethiopia)

Appendix C: Radiometric correction and calibration

The following steps were applied during radiometric calibration of Landsat TM, ETM+ and OLI_TIRS images.

- ✓ Conversion to at-sensor spectral radiance

For visible-red band (band 3), near-infrared band (band 4) and thermal-infrared band (Band 6) of ETM+ and TM imagery, the at-sensor spectral radiance was calculated by the equation (USGS, 2019):

$$L\lambda = \left(\frac{LMAX\lambda - LMIN\lambda}{Qcalmax - Qcalmin}\right) * (\mathrm{Qcal} - \mathrm{Qcalmin}) + \mathrm{LMIN}\lambda \quad (10)$$

where Lλ is at sensor spectral Radiance, LMAXλ is a radiance scaled to QCALMAX), LMINλ is a radiance scaled to QCALMIN), QCAL is the quantized calibrated pixel value in DN , QCALMIN is minimum quantized calibrated pixel value corresponding to LMINλ is 1 and QCALMAX is maximum quantized calibrated pixel value corresponding to LMAXλ is 255(from metadata file).

And also, DN values of the thermal infrared (TIR) (band 10) data of Landsat-8 OLI were converted to Sensor Spectral Radiance by the following equation using rescaling factors provided in the metadata file (USGS, 2016):

$$L\lambda = ML * Qcal + AL \quad (11)$$

Where Lλ is at-sensor spectral radiance, ML is radiance multiplicative scaling factor for the band, AL is Radiance additive scaling factor for the band, Qcal is pixel value in DN.

- ✓ Conversion to Top of Atmosphere (TOA) reflectance

The red and near-infrared bands of ETM+ and TM were converted in to top of Atmosphere (TOA) reflectance by the equation (USGS, 2019):

$$\rho\lambda = \frac{\pi . L\lambda . d2}{ESUN\lambda . cos\ \theta s} \quad (12)$$

where ρλ is planetary TOA reflectance, π is mathematical constant equal to ~3.14159, Lλ is at sensor Spectral radiance, d is earth-sun distance (from metadata file), ESUNλ is Mean exo atmospheric solar irradiance from (Chander et al., 2009), θs is solar zenith angle (90-sun elevation angle) * (180/ π).

In addition, the DN values of the red band (b4) and near-infrared (b5) of OLI were converted to Top of Atmospheric reflectance by the equation (USGS, 2016):

$$\rho\lambda' = M\rho * Qcal + A\rho \qquad (13)$$

where ρλ' is TOA planetary spectral reflectance, without correction for solar angle, Mρ is reflectance multiplicative scaling factor for the band, Aρ is reflectance additive scaling factor for the band, and Qcal is pixel value in DN (from metadata file).

However, ρλ' is not true TOA Reflectance, because it needs additional a correction for the solar elevation angle. The conversion to true TOA Reflectance was calculated by the equation (USGS, 2016):

$$\rho\lambda = \frac{\rho\lambda'}{\sin\theta SE} \qquad (14)$$

ρλ is TOA planetary reflectance, θSE is local sun elevation angle; the scene center sun elevation angle in degrees is provided in the meta data.

- ✓ Conversion to Top of Atmosphere Brightness

The thermal infrared (TIR) band data of TM, ETM+ and Landsat-8 OLI were converted to brightness temperature, which is the effective temperature viewed by the satellite under an assumption of earth's surface is a black body (i.e., spectral emissivity is 1), and includes atmospheric effects (absorption and emissions along path).

Brightness temperature was calculated by the formula (USGS, 2016, USGS, 2019):

$$T_B = \frac{K2}{ln(K1/L\lambda+1)} \qquad (15)$$

where

T_B is Brightness temperature (K), Lλ is TOA spectral radiance, K1 is calibration constant 1, and K2 is Calibration constant 2, (from metadata file).

Appendix D: Climate data consistency test

The double mass curve technique was applied to check and adjust the consistency and homogeneity of temperature and rainfall data in the 16 selected station. In this method a group of neighboring stations are chosen in the vicinity of doubtful station. The cumulative climate data of each doubtful station is plotted against the mean of the cumulative climate data of neighboring stations. A break in the slope of the plot indicates a change in the climate data. This criterion was used in this study to check and adjust the consistency and homogeneity of climate data in the selected station with help of Hydrognomon software. Hydrognomon is capable of performing many of the statistical procedures in hydrology. It is such a powerful tool for double mass curve analysis. In addition to plotting the double mass curve, it is capable of automatically correcting the homogeneity of the time series with respect to a user selected reference station (Kozanis et al., 2005).

The following figures clearly illustrates, climate data of all the stations were found to be consistent for the period of 1989 to 2018 with strong determination coefficient of R^2 value greater than 0.998.

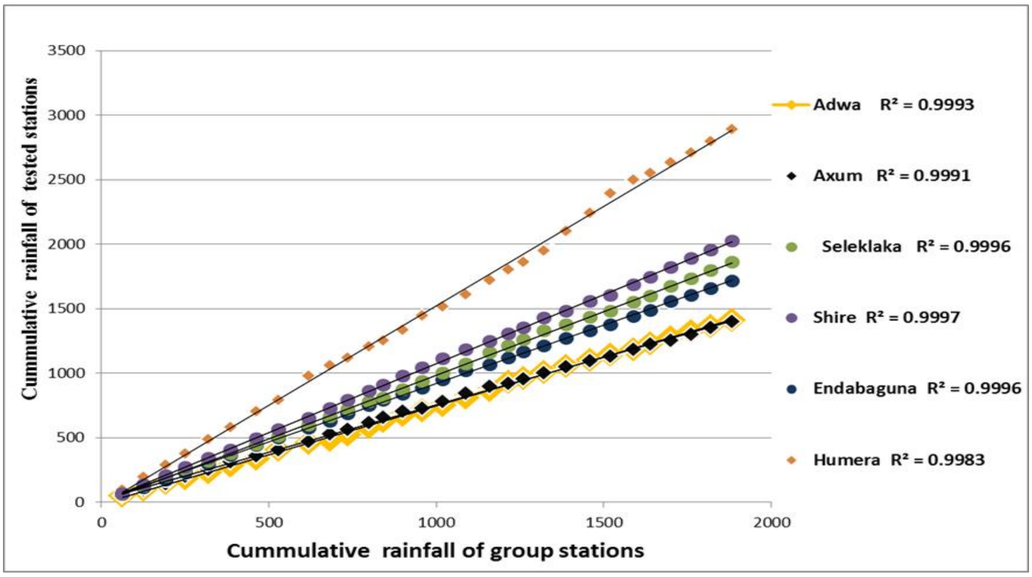

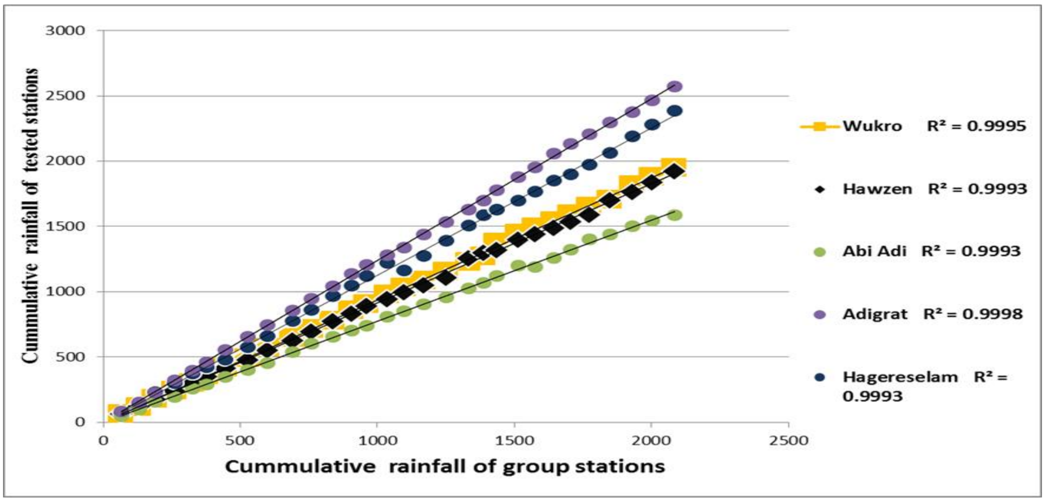
Cummulative rainfall of tested stations
Cummulative rainfall of group stations
Wukro R² = 0.9995
Hawzen R² = 0.9993
Abi Adi R² = 0.9993
Adigrat R² = 0.9998
Hagereselam R² = 0.9993

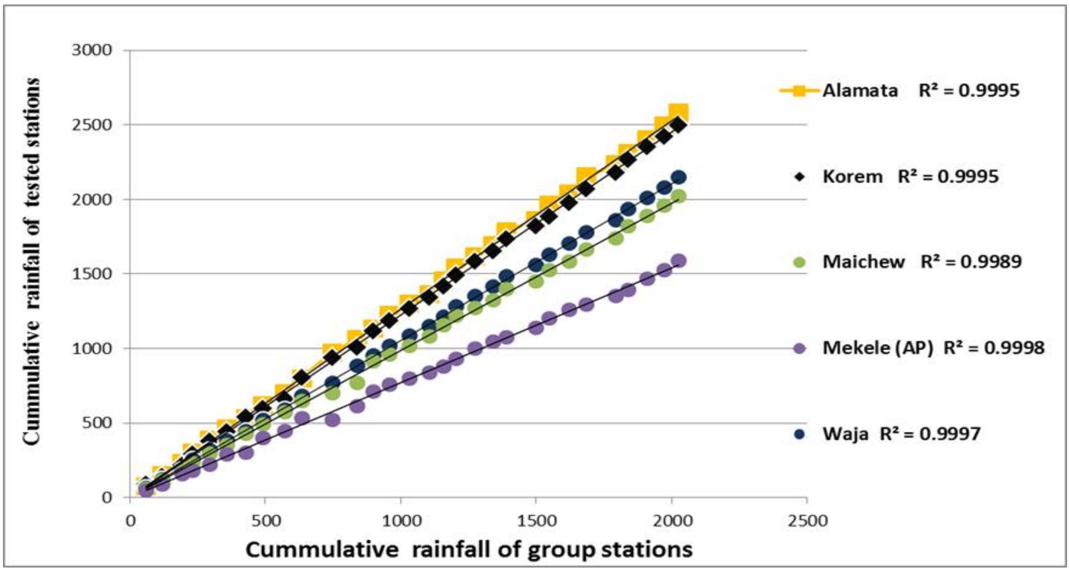
Cummulative rainfall of tested stations
Cummulative rainfall of group stations
Alamata R² = 0.9995
Korem R² = 0.9995
Maichew R² = 0.9989
Mekele (AP) R² = 0.9998
Waja R² = 0.9997

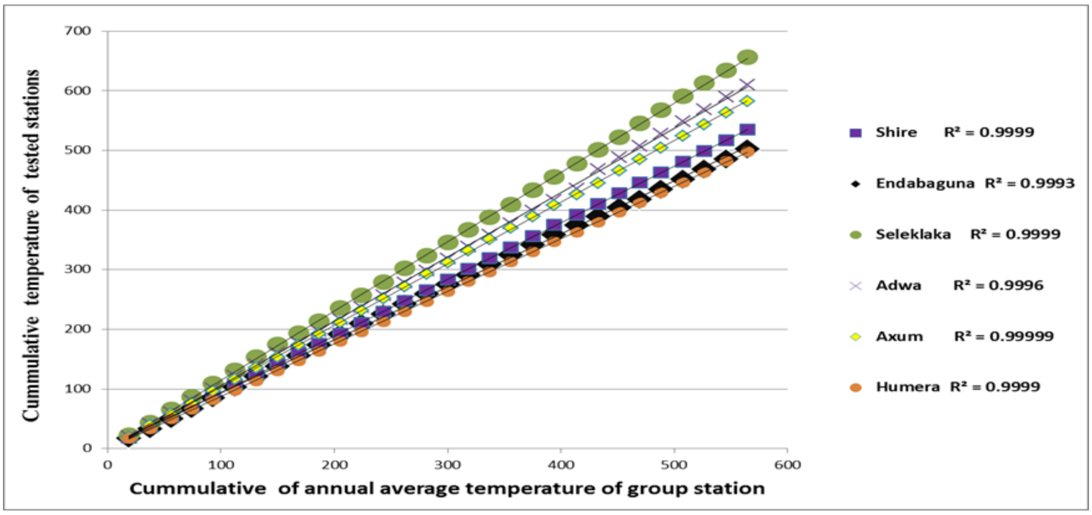
Cummulative temperature of tested stations
Cummulative of annual average temperature of group station
Shire R² = 0.9999
Endabaguna R² = 0.9993
Seleklaka R² = 0.9999
Adwa R² = 0.9996
Axum R² = 0.99999
Humera R² = 0.9999

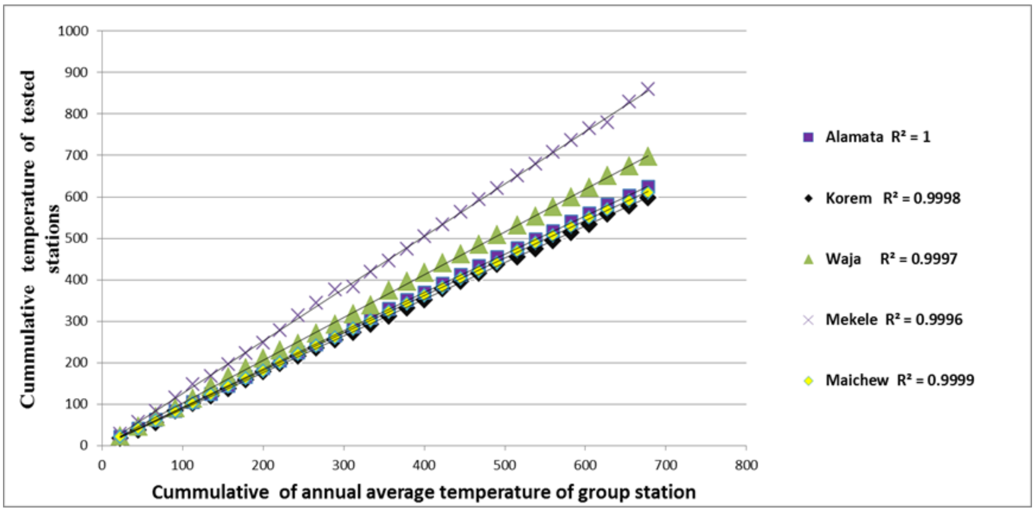

Cummulative temperature of tested stations
Cummulative of annual average temperature of group station
Alamata R² = 1
Korem R² = 0.9998
Waja R² = 0.9997
Mekele R² = 0.9996
Maichew R² = 0.9999

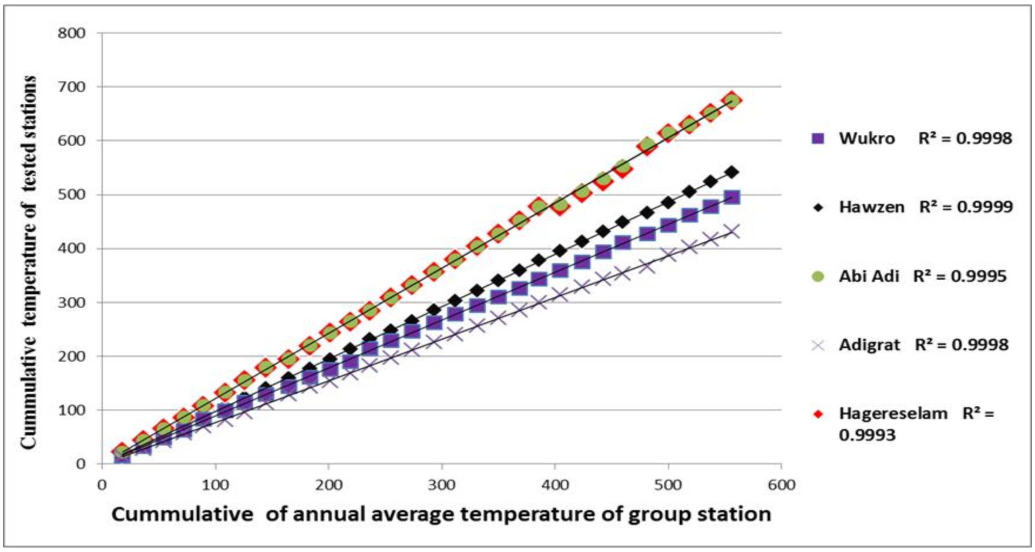

Cummulative temperature of tested stations
Cummulative of annual average temperature of group station
Wukro R² = 0.9998
Hawzen R² = 0.9999
Abi Adi R² = 0.9995
Adigrat R² = 0.9998
Hagereselam R² = 0.9993

Appendix E: Standardized Precipitation and Evapotranspiration Index (SPEI)

The calculation of SPEI required precipitation and potential evapotranspiration as an input.

In this study, first the mean temperature was used to calculate PET (mm) using (Thornthwaite, 1948). The simplest approach to calculate PET is used, which has the advantage of only requiring data on monthly mean temperature.

Following this method, the monthly PET (mm) is obtained by:

$$\mathrm{PET} = 16\mathrm{K}\left(\frac{10\mathrm{T}}{\mathrm{I}}\right)^{\mathrm{m}} \tag{16}$$

where T is monthly mean temperature in degree Celsius; I is heat index derived from 12 monthly index values calculated as a sum of 12 monthly index values i, which is calculated as given in the equation:

$$i = \left(\frac{T}{5}\right)^{1.514} \tag{17}$$

m is a coefficient depending on I, can be calculated as follows

$$m = 6.75 * 10^{-7}I^3 - 7.71 * 10^{-5}I^2 + 1.79 * 10^{-2}I + 0.492 \tag{18}$$

K is a correction coefficient computed as a function of the latitude and month (eq):

$$K = \left(\frac{N}{12}\right)\left(\frac{NDM}{30}\right) \tag{19}$$

where NDM is the number of days of the month and N is the maximum number of sun hours, which is calculated using (equation):

$$N = \left(\frac{24}{\pi}\right)\omega_s \tag{20}$$

where ω_s is the hourly angle of sun rising, which is calculated using (equation):

$$\omega_s = \arccos(-\tan\varphi\tan\delta) \tag{21}$$

where φ is the latitude in radians and δ is the solar declination in radians, calculated using :

$$\delta = 0.4093 \text{sen}\left(\frac{2\pi J}{365}\right) - 1.405 \quad (22)$$

where, J is the average Julian day of the month.

The difference between precipitation and potential evapotranspiration provides a measure of water surplus or deficit for the month and this is compared over time and standardized to get the value of SPEI.

$$d_i = P_i - PET_i \quad (23)$$

d_i is a difference of precipitation and potential evapotranspiration for month i. The probability distribution of cumulative D i is aggregated at different time scales following the same procedure as that for the SPI. The difference D^K i, j in a given month j and year i depends on the chosen time scales, k. In quantifying the SPEI is needed to use a three-parameter distribution, since in two parameter distributions the variable (x) has a lower boundary of zero (0 > x < ∞), whereas in three parameter distributions x can take values in the range (γ > x <∞, where γ is the parameter of origin of the distribution), consequently, x can have negative values, which are common in D series. To model Di values at different time scales are used the probability density function of a three parameter Log-logistic distribution:

$$f(x) = \frac{\beta}{\alpha}\left(\frac{\alpha-\gamma}{\alpha}\right)^{\beta}\left(1 + \left(\frac{\alpha-\gamma}{\alpha}\right)^{\beta}\right)^{-2} \quad (24)$$

where α, β and γ are scale, shape and origin parameters, respectively, for D values in the Range (γ>D<∞). The Log-logistic distribution adopted for standardizing the D series for all time scales is given by:

$$F(x) = \left[1 + \left(\frac{\alpha}{\alpha-\gamma}\right)^{\beta}\right]^{-1} \quad (25)$$

F (x) value is then transformed to a normal variable by means of the following approximation:

$$SPEI = W - \frac{c_0 + c_1 w + c_2 w^2}{1 + d_1 + d_2 w^2 + d_3 w^3} \quad (26)$$

where, $c_{0,} c_1$, c_2, d_1, d_2, $d_3$is similar constants as for SPI and W is probability-weighted moments:

$$W = \sqrt{-2\ln(P)} \tag{27}$$

P≤0.5 and P is the probability of exceeding a determined D value. The average value of SPEI is zero, and the standard deviation is one.